

Blade-Vortex Interaction Noise Characteristics of a Full-Scale Active Flap Rotor

Ram D. JanakiRam
Manager, Flight Technology
The Boeing Company
Mesa, AZ
ram.d.janakiram@boeing.com

Ben W. Sim
UARC
U.S. Army AFDD
Moffett Field, CA
ben.w.sim@us.army.mil

Cahit Kitaplioglu
Aeromechanics Branch
NASA Ames Research Center
Moffett Field, CA
Cahit.Kitaplioglu-1@nasa.gov

Friedrich K. Straub
Boeing Technical Fellow
The Boeing Company
Mesa, AZ
friedrich.k.straub@boeing.com

ABSTRACT

Acoustic measurements of a full-scale active flap rotor obtained from the joint Boeing/DARPA/NASA/Army test in the Air Force National Full-Scale Aerodynamic Complex 40- by 80-foot anechoic wind tunnel demonstrated the potential of active flaps to reduce blade-vortex interaction (BVI) noise over a wide range of directivity angles underneath the advancing rotor disk. The active flap rotor is a full-scale MD 900 helicopter main rotor with all of its five blades modified to include an on-blade piezoelectric actuator-driven flap with a span of 18% radius, 25% chord and located at 83% radius. Results are shown for three simulated descent flight conditions where BVI noise radiation was expected to be dominant for the baseline rotor. The baseline rotor for each test condition was simulated with 0° flap deflections (achieved via closed loop flap position control) on all the blades. For each test condition, open-loop single harmonic flap excitations with varying frequencies (2- to 5-per-rev), input phase and amplitude were used to demonstrate BVI noise reductions. Active flap schedules were identified which showed BVI noise reductions varying from 2 to 7 dB depending on the flight speed. Predictions made with CAMRAD II/PSU-WOPWOP code did not correlate well with active flap test data although the BVI noise levels for baseline rotor were well predicted for the low speed test cases. Hub loads increased for active flap schedules used for BVI noise reduction.

INTRODUCTION

The relatively high noise levels generated by rotorcraft during descent or approach operations around heliports as well as maneuvering rotorcraft operations around military bases are viewed as environmentally unacceptable to the general public particularly in areas where there is high volume air traffic. Increasingly stringent environmental restrictions imposed by federal and municipal regulatory agencies also continue to stunt the growth of short-haul commercial rotorcraft operations. The high noise levels in helicopter descent flight operations as well as maneuvers are caused by an impulsive noise-generating mechanism known as blade-vortex interaction (BVI) that results from the close proximity between a helicopter's main rotor blades and the vortices generated by them during the flight. Over the past two decades, substantial progress was made [1, 2] in understanding the fundamental mechanisms underlying this noise as well as development and demonstration of various rotor source noise reduction and flight path control techniques for reducing the BVI noise on the ground under a helicopter in descent flight. It was established that the rotor BVI noise, when it occurs, is generated by rapid pressure

fluctuations near the blade leading edge due to interaction with the previously generated tip vortices and is strongly influenced by rotor blade tip vortex structure (strength and core radius) and its geometry (vertical separation and angle of interaction) relative to the blade in the interaction region. In descent flight, the forward speed, rotor angular speed and rate of descent affect the geometry of trailed blade wake and rotor blade lift distribution affect the structure of the blade tip vortices. It was shown [3] that parallel and nearly parallel interactions between the blade and the trailed vortices on the advancing rotor blades generate a strong far-field noise radiation pattern, which is mostly forward and underneath the advancing rotor blades.

Various passive blade modifications were conceived and tested in model rotor experiments to reduce the BVI noise in the far field [2, 4, 5, and 6]. Most of these efforts were aimed at redistributing airloads near the blade tip to help modify tip vortex structure or inducing vortex instability and or changing the vertical separation (or miss distance) between the blade and the tip vortex during the interaction. Blade tip sweep is perceived to be effective in reducing BVI noise by avoiding or delaying parallel blade vortex interactions. Blade tip modifications considered included swept- tapered tip, an Ogee tip, parabolic tip, anhedral and BERP tips. Limited BVI noise reduction was demonstrated in model rotor experiments and flight tests

with these blade tip modifications [4, 6]. Some modern helicopters such as MD 900, EC 145, S-92 and EH-101 have incorporated some of these blade tip shapes. Any passive modification to the blade to affect BVI noise will also have an impact on aerodynamic performance and vibratory loads sometimes adversely. This led to the exploration of active rotor control as a means of reducing of BVI noise. The idea here is to invoke the active control only under conditions where BVI noise radiation is strong such as in descent flight.

The first active rotor control investigated for BVI noise reduction was with higher harmonic control (HHC) of blade root pitch [7, 8]. In this technique, the blade pitch angle is excited at higher harmonic frequencies (for an N bladed rotor at frequencies corresponding to N , $N-1$ and $N+1$ times the rotor rotational frequency) at a selected amplitude and phase through actuators placed under the rotor swash-plate. This higher frequency pitch excitation along with the trimmed blade pitch schedule (collective and cyclic) seeks to modify the blade lift distribution around the rotor azimuth resulting in modified blade flapping, tip vortex structure and wake trajectories. It was shown through model rotor wind tunnel tests in an acoustic tunnel [7, 8] that for certain open loop HHC blade pitch schedules (amplitude, frequency and phase), rotor BVI noise is reduced by as much as 6 dB. This noise reduction manifests itself as reduction in spectral levels at higher harmonic blade passage frequencies (typically 6 to 50). It was theorized based on detailed wake and other measurements in model rotor wind tunnel tests [9, 2] that for HHC inputs for low noise, blade airloads are modified resulting in a new wake structure (strength and trajectory) of the blade tip vortex and blade flapping. This, it is postulated, results in a substantial increase in the blade-vortex miss distance and perhaps blade-vortex interaction angle leading to a reduction in BVI noise. The HHC rotor wind tunnel tests [7] have also shown that the HHC inputs for low noise have substantially increased rotor hub vibratory loads.

In order to increase control flexibility, an individual blade control (IBC) technique wherein the pitch links in the rotating system are replaced by hydraulic blade pitch actuators, was devised to actively control rotor vibratory loads and BVI noise. This IBC allows for an arbitrary blade pitch variation. Full-scale wind tunnel tests and flight tests were carried out for a BO-105 rotor with an IBC system [10, 11]. These tests have demonstrated that BVI noise and vibratory loads can be simultaneously reduced with multiple harmonic inputs and 2-per-rev control holds promise for flight performance improvements in high-speed flight. Rotor BVI noise reductions of the order of 12 dB in wind tunnel tests and about 5 dBA in flight tests were measured [10, 11]. A closed-loop BVI noise controller based on feedback from skid-mounted microphones on a BO-105 helicopter with an IBC system on its main rotor was successfully used to demonstrate BVI noise reductions on the ground under its flight path [12]. BVI noise reductions were also demonstrated on wind tunnel tests of a full-scale UH-60 rotor [13] with an IBC system. The IBC rotor

systems, however, suffer some major drawbacks, which include high actuator power required to control the full-blade and mechanical complexity of the hydraulic pitch link actuators and the need for fail safe operation since they are part of the primary control system load path. This led to the exploration of smart on-blade structures for active rotor control such as piezo-actuated blade trailing edge flaps and active blade twist using embedded piezo-ceramic materials. A model scale active twist rotor with embedded active fiber composite actuators was recently tested in a wind tunnel to demonstrate BVI noise and vibratory loads reductions [14]. The BVI noise reduction results were not as promising as those from HHC and this concept also suffers from the need to deform the full blade with higher actuator power.

Active rotor control with blade trailing edge flaps for vibration and BVI noise reduction has certain advantages especially when compared to root pitch actuation systems. First, the control can be accomplished using suitably located trailing edge flaps over a small portion of the outboard blade and thus requiring relatively low actuator power, loss of functionality of these flaps is not deemed to be as critical since they are not part of the primary control system and the use of electric power to actuate the flaps instead of hydraulic power is considered less mechanically complex and more reliable. One of the first early attempts of active control of trailing edge flaps for BVI noise reduction involved the wind tunnel test demonstration of a rotor with mechanically driven non-harmonic trailing edge flap control [15]. This test showed the potential of at least 4 dB BVI noise reductions. Over the past few years there have been several significant analytical and experimental efforts to demonstrate the high potential of active flap rotors for BVI noise and vibratory hub loads reduction [16-20]. It was shown through computational studies [19] that the active flap control is effective for advancing-side BVI noise reduction both in the near-field and far-field and that open-loop inputs that are most effective for BVI noise reduction are not the same as that for effective vibration reduction. However, it was also shown that the active flap system is capable of simultaneous noise and vibration reduction [18]. In recent years, blade trailing edge flap system actuated by in-blade smart material actuators have emerged as a primary candidate.

Full-scale rotors [21-24] with piezo-electric actuated blade trailing edge flaps were designed, built and tested in whirl tower and flight tests. Eurocopter has conducted design studies to determine the size and placement of a blade trailing edge flap system on the main rotor of a BK-117 helicopter [23]. A trade-off between two working mechanisms associated with flap system was considered [23]; a direct lift generation by flap incidence angle affecting the camber of the blade sections (downward flap deflection increases the lift, generally associated with larger flaps and stiffer blades) and an indirect lift generation by elastic twist of the blade through the pitching moment generated by the flap (downward flap deflection introduces nose down pitching moment leading to a nose down elastic twist and lower lift – known as servo effect). For noise control,

optimum radial position was estimated to be as near as possible to the blade tip whereas for vibration control, a more inboard flap position was more efficient. Smaller flap chord ratios (15%) were preferred as a compromise between control efficiency and required actuator power. Flight tests of a BK-117 helicopter with the active blade trailing edge flap system showed large reductions in hub vibratory loads and fixed system (gearbox) vibrations [24]. BVI noise reductions are not yet reported.

ACTIVE FLAP ROTOR SYSTEM

Boeing, under the sponsorship of DARPA, NASA, Army and its internal funds has, over the past years, developed an active flap rotor system (alternatively referred to as SMART (Smart Material Actuated Rotor Technology) rotor system) with on-blade piezoelectric-actuated trailing edge flap on each blade of a full-scale five-bladed MD 900 helicopter rotor. The objective of the development of this rotor system is to demonstrate significant rotor-induced vibration and BVI noise reductions in full-scale wind tunnel and flight tests. Reference 25 provides details on the design, development and testing of this active flap rotor system.

Rotor and Flap Characteristics

The SMART rotor (Fig. 1) is a 33.85-ft diameter (blade radius, R of 203.1 inches), full-scale, bearingless, five-bladed main rotor modified from existing MD 902 Explorer rotor system. Each blade consists of HH-10 airfoil (12% thick) sections inboard (up to 74% radius) and HH-06 (9.5% thick) airfoil sections outboard (beyond 84% radius), with a linear twist of -10 degrees. The blade tip region, from 93% radius to the tip has a parabolic leading edge sweep (22 degrees at the tip), straight trailing edge and a 2:1 taper ratio. The constant chord section of the blade is 10 inches long. Nominal rotation speed of the rotor is 392 RPM producing a tip speed of 695 ft/sec. At 5,811 pounds thrust, the rotor thrust coefficient normalized by thrust-weighted rotor solidity is 0.075 at sea level standard conditions.

Rotor Characteristics	
Rotor Blade	Modified MD900
Hub Type	Bearingless
No. of Blades	5
Blade Radius	203.1 inches
Rotor Speed	392 RPM
Tip Chord	10 inches
Airfoil	HH-10, HH-06
Twist	10 deg.

Trailing-Edge Flap Data	
Radial Station	150 - 186 inches
Length	36 inches
Chord	3.5 inches
Hinge Location	75% Chord
Max. Flap Angle	± 6 deg.

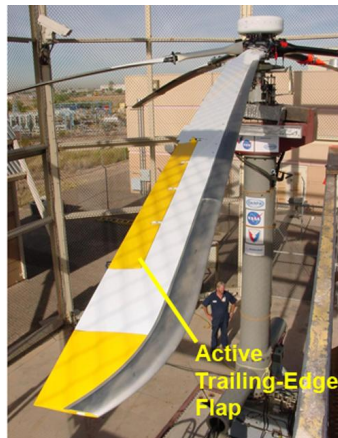


Figure 1. Boeing-SMART Rotor with active trailing edge flap

Of particular interest here is the design of the flap system and its integration into the MD 900 rotor blades. Aerodynamic and aeroelastic simulations were conducted early [26] on to define the flap type, flap chord and flap span such that the flap system has enough control authority to provide required dynamic lift variations for vibration and noise reduction and requires the minimum actuator power. The flap system selected [25] has a flap/chord ratio of 25% with an overhang of 40% (total flap length of 35% chord) and flap span of 18% rotor radius with its center located at 83% rotor radius [25] to provide required control authority while minimizing the flap hinge moments and stresses. Each blade contains an embedded piezoelectric actuator designed to drive the trailing edge flap at frequencies from one-per-rev (2P) up to eleven-per-rev (6P), with as much as 6° amplitude, depending on the harmonic frequency. Inputs to the five blades are phased azimuthally such that each flap receives the same command at a given azimuth. The piezoelectric actuator is installed in the blade spar at 74% radius. It drives the flap via a linkage that is connected to a horn at the inboard end of the flap. Reference 25 provides more details, on the piezoelectric actuator development and its integration into the rotor blade. Equation 1 shows the mathematical representation of a flap actuation with deflection angle (δ_f) prescribed as a function of the blade azimuth (ψ), active flap amplitude (A_f), normalized harmonic frequency (H_f) and phase (ϕ_f). Positive deflection angles relate to flap down positions. For the rest of this paper, active flap settings will be described in a three-parameter form, $A_f/H_f/\phi_f$ – where A_f and ϕ_f are expressed in degrees and H_f is the normalized harmonic frequency expressed as integer multiple of the rotation frequency.

$$\delta_f = A_f \cdot \sin(H_f \psi + \phi_f) \quad (\text{Eqn. 1})$$

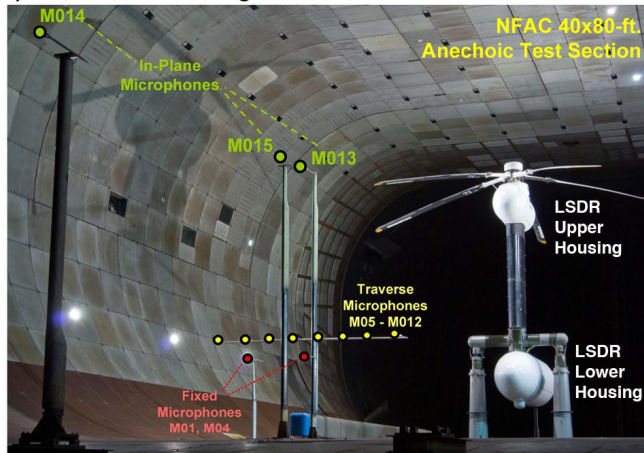
ACTIVE FLAP ROTOR WIND TUNNEL TESTS

Under a joint DARPA/NASA/Army-funded program, Boeing and a team from Air Force, NASA, Army, Massachusetts Institute of Technology, University of California at Los Angeles, and University of Maryland have recently completed a successful wind-tunnel test of the SMART rotor in the 40- by 80-foot wind tunnel of the Air Force National Full-Scale Aerodynamic Complex (NFAC) at NASA Ames Research Center. The eleven-week wind tunnel test program [27] evaluated the forward flight characteristics of the full-scale active-flap rotor and quantified the effects of open- and closed-loop active-flap control on rotor loads, noise, and performance. The test demonstrated on-blade smart material control of flaps on a full-scale rotor for the first time in a wind tunnel. The effectiveness and the reliability of the flap actuation system were successfully demonstrated in more than 60 hours of wind tunnel testing.

Instrumentation

The Boeing-SMART rotor was supported on top of the Large Rotor Test Stand (LRTS) when installed in the NFAC 40- by 80-foot test section (Figure 2a). The LSDR consists of an upper and lower housing connected by a vertical stand strut. In the upper housing, the rotor hub is connected to a static mast, which was mounted to a five-component rotor balance. The static mast encloses the rotating drive shaft that transfers torque directly to the rotor hub. In addition, the upper fairing also encloses the balance housing and the hydraulic servo-actuators for the rotor control system. A vertical stand strut connects the upper balance housing to the lower housing that encloses the transmission and a 1,500-hp General Electric motor. The LSDR was mounted in the wind tunnel on a three-strut support system placing the rotor hub 23.7 ft above the tunnel floor at zero degree shaft tilt. Rotor instrumentation includes a five-component balance, drive-shaft torque, and control-system motions.

a) SMART Rotor Testing in NFAC



b) Microphone Layout (Top View)

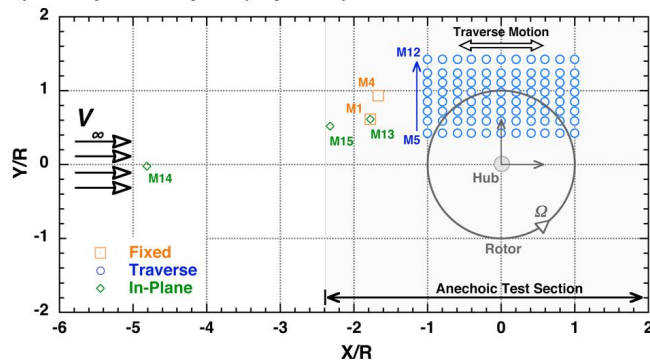


Figure 2. Test setup: a) Boeing-SMART rotor installation in wind tunnel, b) microphone layout

For acoustic measurement, a series of microphones was strategically placed around the model to capture rotor noise sources of interest (Figure 2a). These microphones were grouped into: a) out-of-plane fixed microphones (M1 and M4) to correlate to microphones used previously in the MDART test [28] b), traverse microphones (M5 through M12) that can be moved along guided rails for blade-vortex interaction noise mapping and c) in-plane microphones (M13, M15 and M14) for low frequency, in-plane rotor noise measurement. Microphones M13, M15 and M14 were mounted on tower struts to be near in-plane of the rotor (approximately 10 degrees below wind tunnel horizon). With the exception of M14, all microphones are located within the acoustically-treated portion of the 40- by 80-foot test section. Summaries of the microphone positions, relative to both the rotor hub are illustrated in Table 1a. Of particular interest to establish the BVI noise characteristics of the active flap rotor system are the array of traverse microphones and the traverse stations upstream and downstream of the hub center. The traverse travel ranges from 200 inches (98.5% rotor radius) upstream of the center of the rotor hub to 200 inches downstream with traverse stopping at every 40 inches (Fig. 2b). Acoustic data acquisition at the traverse array of microphones at each of these traverse locations will help establish the noise characteristics over a plane of microphones located 89.4% radius below the rotor hub center underneath the advancing side extending from 41% radius to 141% radius on the starboard side and 98.5% radius upstream to 98.5% downstream (Fig. 2b). These microphone locations cover a wide range of out-of-plane directivity angles underneath the advancing rotor disk. Table 1a provides the directivity angles (Θ , elevation angle below the rotor disk and Ψ , azimuthal angle) for all the microphones including those on the traverse when it is located at the farthest upstream position (i.e. traverse station: -200). Table 1b shows the traverse stations used in the test to cover the spatial positions where BVI noise radiation is likely to be the strongest, underneath the advancing side of the rotor. Retreating side BVI noise characteristics were not measured in this test since a microphone traverse could not be placed on the retreating side of the rotor due to logistical reasons.

Instrumentation-grade 1/2-inch free-field condenser microphones (G.R.A.S. Type 40AC) with nose cone fairings were used in the acoustic measurement. Microphone signals were pre-amplified at the source to minimize signal loss over the long wiring runs leading to a junction box housed below the test section - from which the signals were sent to both an acoustic monitoring station and to the data acquisition console. Microphone gains were adjusted at the monitoring station on a per-test point, per-channel basis to maximize signal-to-noise ratio. In addition to the microphone signals, encoders on the rotor shaft provided a one-per-rev trigger signal, as well as a 256-per-rev and a 2048-per-rev sampling clock.

Table 1a. Microphone positions (hub-centered, 0° shaft tilt)

Sensor Name	Cartesian ¹			Spherical ²				Notes
	X, ft	Y, ft	Z, ft	r, ft	r/R	Ψ , deg	Θ , deg	
M01	-29.67	10.27	-17.94	36.16	2.14	160.9	-29.7	Fixed Microphones
M04	-27.92	15.59	-17.87	36.63	2.16	150.8	-29.2	
M05	-16.73	6.97	-15.13	23.61	1.39	157.4	-39.9	Traverse Microphones (station: -200)
M06	-16.73	9.79	-15.13	24.59	1.45	149.7	-38.0	
M07	-16.73	12.02	-15.13	25.56	1.51	144.3	-36.3	
M08	-16.73	14.17	-15.13	26.64	1.57	139.7	-34.6	
M09	-16.73	16.42	-15.13	27.90	1.65	135.5	-32.8	
M10	-16.73	18.67	-15.13	29.28	1.73	131.9	-31.1	
M11	-16.73	20.90	-15.13	30.75	1.82	128.7	-29.5	
M12	-16.73	23.92	-15.13	32.88	1.94	125.0	-27.4	
M13	-29.67	10.27	-5.34	31.85	1.88	160.9	-9.7	In-Plane Microphones
M14	-38.77	8.73	-7.13	40.38	2.39	167.3	-10.2	
M15	-80.36	-0.33	-14.84	81.72	4.83	180.2	-10.5	

Note 1 (tunnel-axis)

X – positive towards aft of rotor

Y – positive towards starboard

Z – positive up

Note 2

r/R – hub-to-microphone distance, non-dim. by rotor radius, R

 Ψ – azimuth angle (0° aft, counter-clockwise) Θ – elevation angle (0° in horizon plane, positive up)**Table 1b. Microphone traverse stations¹**

Station	X, ft	X/R	Notes
-200	-16.73	-0.988	Forward of rotor
-160	-13.33	-0.788	
-120	-10.00	-0.591	
-80	-6.67	-0.394	
-40	-3.33	-0.197	
0	0	0	Aligned with rotor hub
+40	3.33	0.197	Aft of rotor
+80	6.67	0.394	
+120	10.00	0.591	
+160	13.33	0.788	
+200	16.73	0.988	

Note 1 (tunnel-axis)

X – positive towards aft of rotor

Data Acquisition

With the exception of wind tunnel test conditions and acoustic measurements, all rotor and active flap control were recorded on Boeing's time-based sampling data acquisition system. For each test point, sixty-four revolutions of data (approximately 9.8 seconds) were collected to enable time-domain averaging on a rotor revolution basis. All channels, except those corresponding to acoustic measurement, were post-processed to 256 samples per revolution using the sampling clock from the rotor encoder. The acoustic data channels were digitized at an effective sampling rate of 2048 samples/revolution (equivalent to 13,380 samples/sec at the nominal 392 RPM). Sixty-four revolutions of data were digitized at each test condition. The data exhibited good rev-to-rev repeatability; therefore, a straightforward synchronous average of the time history data resulted in an averaged time history of one revolution duration of 2048 points. The Fourier transform of this averaged time history yielded a power spectrum of one-per-rev resolution (6.53 Hz for 392 RPM). The averaged time history was band-pass filtered

between the 8th and 60th blade-passage harmonics to focus on the BVI event. These limits were selected based on the criterion of best preserving the BVI pulse characteristics such as peak-to-peak level, pulse slope, and pulse width. Two noise level metrics were obtained by integrating the respective sound pressure power spectra; OASPL from the overall unfiltered spectra and BVISPL from the bandpass-filtered spectra. The NFAC acoustic data acquisition and reduction system enabled the near real-time acoustic processing of the data. The BVISPL and OASPL levels were made available for all the microphones within a few seconds of data acquisition.

Acoustics Tests













One of the primary objectives of the wind tunnel test program was to establish the noise reduction potential of the active flap rotor. A companion paper [29] discusses the in-plane, low frequency noise characteristics of this full-scale active flap rotor. Here we focus on the BVI noise

characteristics for three simulated steady state descent flight test conditions of an MD 902 helicopter where BVI noise radiation is expected to be strongest. All acoustic tests were conducted at a nominal thrust coefficient-to-solidity ratio (C_T/σ) of 0.075 (which corresponds to 5811 pounds of rotor thrust at sea level, standard day conditions) and a rotor tip Mach number (M_{tip}) of 0.623 which corresponds to seal level, standard conditions. . The first series of tests were conducted at an advance ratio (μ) of 0.150 (forward speed of approximately 62 knots). At this low speed condition with aft (positive) rotor shaft tilt (α) to simulate descending flight, BVI noise is expected to dominate the out-of-plane noise radiation. The second series of tests were conducted at a forward speed of 68 knots, ($\mu = 0.165$) and a shaft angle setting of $+1.8^\circ$ aft, which is estimated to simulate the FAA noise certification flight test condition (6° glide-slope) of an MD 902 helicopter. In this series, the rotor RPM of 392 was maintained constant which led to an M_{tip} of 0.617 on the test day. The third and final series of tests were conducted at a forward speed of 82 knots ($\mu = 0.200$) to establish the effects of relatively high forward speed on BVI noise. Effects of active flap on BVI noise were systematically studied via phase and amplitude sweeps at various flap actuation frequencies.

For all the test cases, the following procedure was used to establish the BVI noise characteristics of the active flap rotor. For each test condition, rotor was trimmed to the desired thrust and minimal hub moments prior to active flap

excitation, and was not re-trimmed during subsequent phase and amplitude sweeps. At all test conditions, BVI noise characteristics were first established for the baseline condition where the flaps are not actuated. Majority of the test points were obtained with closed-loop (flap position) control, with the exception of some baseline cases at the beginning of the test program that were performed with open-loop flap position control. For the first and third series of tests (μ of 0.150 and 0.200), shaft angle sweeps were conducted to identify the shaft angles corresponding to maximum BVI for the baseline rotor at the selected microphone locations. Once the shaft tilt for maximum BVI was identified for the baseline rotor, a traverse sweep was conducted to identify the microphone location(s) on the traverse sweep where BVISPL noise level is the highest. With the traverse parked at the microphone location corresponding to maximum BVISPL level, open-loop flap inputs (amplitude, input phase and frequency sweeps) were conducted to identify the combination of active flap parameters for maximum BVI noise reduction. Once these were identified, a traverse sweep was conducted to establish the BVI noise characteristics of the active flap rotor. Same procedure was used for the second test case of μ of 0.165 except that no shaft angle sweeps were conducted. No closed-loop BVI noise control was attempted in this series of tests. A summary of the test points, used in this paper, and their corresponding operating conditions, is illustrated in Table 2.

Table 2. Boeing-SMART Rotor BVI noise testing

Test Description	Advance Ratio, μ	Shaft Tilt, α , $^{\circ}$	Thrust-Coeff., C_T/σ	Rotating Tip Mach No., M_{tip}	Active Flap Control Inputs				Traverse Station
					Type ¹	Amplitude	Freq.	Phase	
Test Case 1									
• Shaft tilt sweep	0.150	-10.0 - +7.5	0.075	0.623	OL	0 V			-200
• Baseline traverse sweep	0.150	+4.0	0.075	0.623	CL	0.0 $^{\circ}$			-200 - +200
• Active flap freq./phase sweep					CL	1.5 $^{\circ}$	2P - 5P	0 $^{\circ}$ - 360 $^{\circ}$	-120
• Active flap amplitude sweep - best freq./phase					CL	1.0 $^{\circ}$ - 2.0 $^{\circ}$	4P	30 $^{\circ}$.	-120
• Active Flap traverse sweep - best amplitude/freq./phase					CL	1.5 $^{\circ}$	4P	30 $^{\circ}$.	-200 - +200
Test Case 2									
• Baseline traverse sweep	0.165	+1.8	0.075	0.617	CL	0.0 $^{\circ}$			-200 - +200
• Active flap freq./phase sweep					CL	1.5 $^{\circ}$	3P, 4P	0 $^{\circ}$ - 360 $^{\circ}$	-80
• Active flap amplitude sweep - best freq./phase					CL	1.0 $^{\circ}$ - 2.0 $^{\circ}$	3P	180 $^{\circ}$.	-80
• Active Flap traverse sweep - best amplitude/freq./phase					CL	1.5 $^{\circ}$	3P	180 $^{\circ}$.	-200 - +200
Test Case 3									
• Shaft tilt sweep	0.200	-10.0 - +7.5	0.075	0.623	OL	0 V			-200
• Baseline traverse sweep	0.200	+2.0	0.075	0.623	CL	0.0 $^{\circ}$			-200 - +200
• Active flap freq./phase sweep					CL	1.5 $^{\circ}$	2P - 5P	0 $^{\circ}$ - 360 $^{\circ}$	-40
• Active flap amplitude sweep – best freq./phase					CL	1.0 $^{\circ}$ - 2.5 $^{\circ}$	3P	180 $^{\circ}$.	-40
• Active Flap traverse sweep – best amplitude/freq./phase					CL	1.5 $^{\circ}$	3P	180 $^{\circ}$.	-200 - +200

Note 1: OL – Open-loop control (voltage input), CL – Close-loop control (flap deflection command)

BVI sound measurement quality in the 40- by 80-foot test section is facilitated by the 42-inch deep acoustic panels [30] with sound absorption capabilities of 94% or more between 100 Hz and 2,500 Hz at most places in the test section [31]. This is well suited for capturing the SMART Rotor's BVI noise frequencies previously established to be from 8th blade passage frequency (261 Hz) to 60th blade passage frequency (1960 Hz). As such, the BVI acoustic data are deemed representative of free field conditions.

Another factor that raises sound quality measurement concerns is the amount of ambient noise level present during "wind-on" conditions. Typically, ambient noise is dictated by the facility's fan drive system [32], but can include tonal/broadband sounds generated by hydraulic systems and flow-induced sounds from rotor test stand, wind tunnel surface or acoustics apparatus, such as microphone strut and/or microphone body. Figure 3 presents sound time history and frequency spectrum data for Test Case 1 at microphone M09 (traverse station: -200). Representative ambient noise levels measured at microphone M09 are indicated by dotted lines in Figure 3. These ambient noise levels were obtained at 62 knots wind speed ($\mu = 0.150$), with a rotating bare hub (without blades) operating at the nominal rotor RPM of 392. Compared to the Boeing-SMART rotor in baseline configuration (Fig. 3a), excellent signal-to-noise ratios of 20 dB or greater were observed. As

shown in Figure 3b, even for an active flap case where BVI noise is reduced, signal-to-noise ratios remains to be 10 dB or higher. Similar results are found at the higher advance ratios of 0.165 and 0.200.

BVI NOISE PREDICTIONS

Results for SMART Rotor Blade-Vortex Interaction (BVI) noise predictions are also included in this paper. Aeromechanics modeling is obtained from CAMRAD-II [33] to simulate steady-state response of an isolated rotor operating in the wind tunnel. Within the analysis, CAMRAD-II couples blade structural dynamics, rotor wake, blade aerodynamics and flight dynamics to obtain the blade airloads/motions associated with the "trim" state of the rotor. For the purpose of simulating SMART rotor operations during wind tunnel testing, CAMRAD-II is configured to trim to a pre-defined rotor thrust with zero longitudinal and zero lateral blade flapping.

Modeling of the blade structural properties in CAMRAD-II are based on a series of span-wise distributed nonlinear beam finite elements. Each beam element is represented by a full range of fully-coupled blade motions, which includes axial, lead-lag, flapping and torsion, to characterize the elastic behavior of the rotor blade. Effects of the trailing edge flap are locally accounted for via span-wise changes in blade stiffness and blade mass properties.

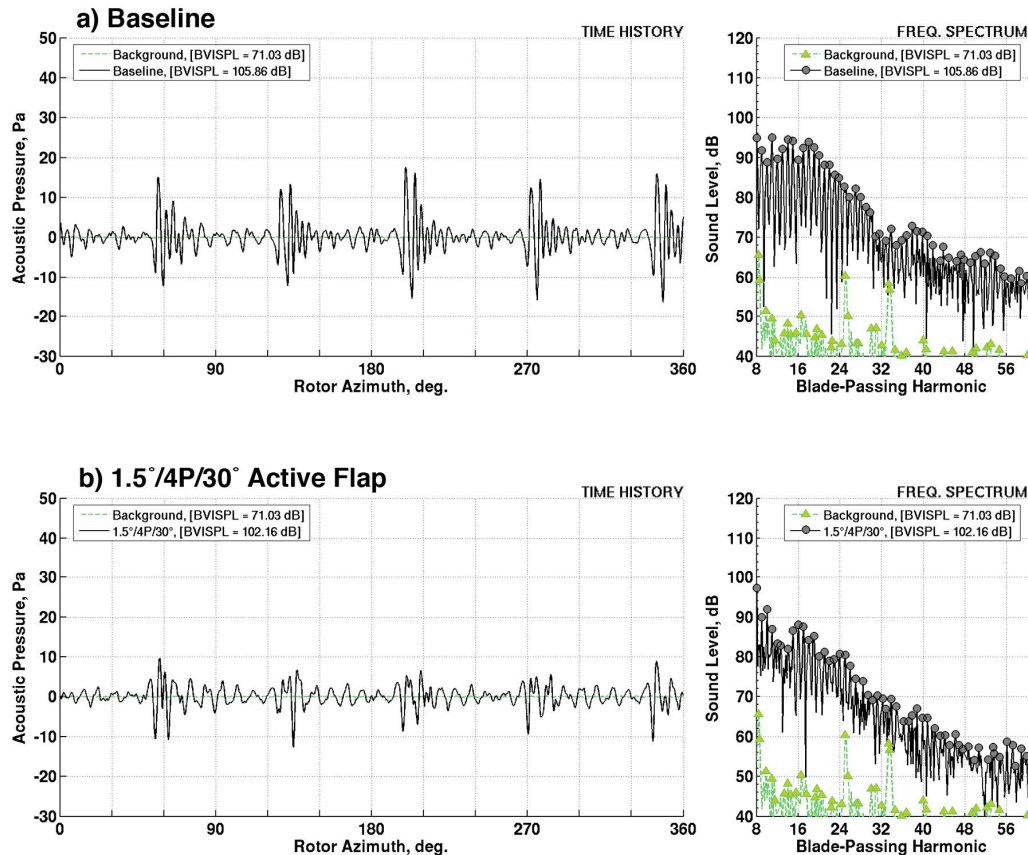


Figure 3. 64 revolutions-averaged rotor and ambient noise time histories, and corresponding spectra for Test Case 1 ($\mu = 0.150$, $\alpha = +4.0^\circ$) at microphone M09 (traverse station: -200); a) baseline rotor, b) active flap rotor 1.5°/4P/30°

The aerodynamic model uses a free-wake analysis to calculate rotor non-uniform induced velocities. The free-wake model consists of a rolled-up wake model [34] based on the formation of a single concentrated tip vortex formed at the blade tip due to span-wise variations in the blade bound circulation. For low speed BVI conditions studied in this paper, the bound circulation is assumed to have the same sign all along the blade span with a single peak location that dictates the vortex strength and roll-up position of the trailed tip vortex. Upon release into the fluid medium, the tip vortex element associated with each time step is modeled as a line segment with a constant core radius of 20% tip chord. Current analysis utilizes up to three revolutions of the rotor wake to capture all pertinent blade-vortex interactions. The inboard shed and trailed vorticity was modeled in a fashion consistent with the rolled-up tip vortex model. Effects of the root vortex and additional trailed vortices introduced by active flap excitations are, however, not considered in present calculations.

Local blade aerodynamics are accounted for using a second-order lifting line model, including effects of the wake-induced velocities, compressibility, yawed flow, blade sweep, Reynolds number, reverse flow and dynamic stall. Blade aerodynamic surfaces are represented by twenty panels located from $0.15R$ to the tip, with panel widths varying from $0.10R$ inboard to $0.02R$ at the tip. These panels are more densely distributed at the outboard (tip) region of the rotor blade to accurately simulate the dominant region important for sound radiation. The static terms of the airloads are computed using airfoil tables, which account for steady viscous and compressible loads. Unsteady lift and moment in the attached flow are calculated based on compressible thin-airfoil theory. Provisions for modeling trailing edge flap aerodynamics were incorporated via an extension of the airfoil tables to include flap angle as an input parameter. An empirically-based Mach number correction [35] is incorporated to better correlate to measured torsion and flap bending loads. This correction is applied only at the blade tip region (from 74% blade radius to the tip) to account for compressibility effects.

All of the predicted aeromechanic airloads and motions are initially computed at a resolution of 15° azimuthal (time) step deemed adequate for rotor trim calculations. A “post-trim” procedure is used to obtain higher resolution airloads and blade motions required for acoustic computations. The “post-trim” procedure makes use of the blade motion and rotor wake model derived from the last trim iteration to determine blade airloads at smaller time intervals corresponding to every 2° azimuth.

The high-resolution airloads and blade motions are passed into PSU-WOPWOP [36] to generate time domain-based acoustics predictions reported in this paper. The acoustic equation, Farassat’s Formulation 1A is implemented in PSU-WOPWOP to relate the blade

geometry and predicted airloads to acoustic pressures in both the near and the far-field. PSU-WOPWOP is configured to simulate a single isolated rotor operating in a steady wind tunnel environment. Because only low-speed BVI conditions are considered in this paper, only the linear thickness noise source and “on-surface” loading noise source terms are included in the acoustic modeling. Non-linear quadrupole effects commonly associated with High-Speed Impulsive (HSI) noise radiation at higher advancing tip Mach number are excluded. In addition, microphone positions in the wind tunnel are assumed to be in close enough proximity to the rotor such that atmospheric propagation effects are negligible.

RESULTS & DISCUSSION

The following section reports the BVI noise characteristics of the active flap rotor at three different test conditions covering a range of simulated low speed descent flight conditions. Results with active flap excitations are compared to the baseline rotor (no flap actuation) to establish the noise reduction potential of the active flap system. The noise data is presented in the form of BVISPL carpet plots underneath the advancing disk. For selected microphone locations, pressure time histories for one revolution of the rotor as well as corresponding spectral data are presented.

Test Case 1: $\mu = 0.150$, $C_T/\sigma = 0.075$, $M_{tip} = 0.623$

This case corresponds to a low speed flight condition (62 knots tunnel speed) where rotor BVI noise can be dominant depending on the shaft tilt. In order to establish the noise reduction potential of the active flap system, a maximum BVI noise condition for the baseline rotor was first identified through a shaft angle sweep. It should be noted that the baseline rotor condition here was simulated using zero voltage input to the flap actuators on all the blades. Figure 4 shows the variation of BVISPL with shaft tilt at microphone M07, traverse station -200 (located $0.985R$ upstream of the rotor hub center). Table 1 provides the location of microphone relative to the hub center for zero shaft tilt. This microphone location is deemed representative for the identification of the shaft angle for maximum BVI noise. As expected, the aft (positive) shaft tilts which correspond to simulated descent flight conditions generated high BVISPLs. Based on this data, the aft shaft tilt angle of 4° was selected for evaluation of the BVI noise characteristics at this forward speed.

It was soon realized that the simulation of baseline rotor condition with (open loop) zero voltage to all the five blade actuators is not an adequate representation of the baseline rotor and that blade flaps are deflecting under the influence of air/inertail loads. Figure 5 shows the trailing edge flap deflection time history during a rotor revolution for each of the five blades with zero flap excitation voltage. It can be clearly seen that with zero voltage excitation some of the

blades are deflecting as high as 0.9° during the rotor revolution and it varied from blade to blade with blade 3 flap showing the lowest flap deflections (less than 0.2°). A closed-loop flap position control was implemented [27, 37] to ensure that the flaps on all the five blades deflect per the commanded harmonic variation (see equation 1) which in the case of baseline rotor is zero flap deflection during the entire revolution. Figure 5 shows that with the implementation of closed-loop position control, for the baseline rotor, all the five blade flaps have nearly zero deflections over the entire rotor azimuth (with a small scatter of 0.04°). Figure 6 shows the difference in time histories and spectral data for the zero voltage and zero flap angle (with closed-loop position control) representations for the baseline rotor at microphone M07 (traverse station: -200) for 4° aft shaft tilt condition. A BVISPL difference of 2.65 dB was measured. All the subsequent noise measurements were taken with closed-loop flap position control.

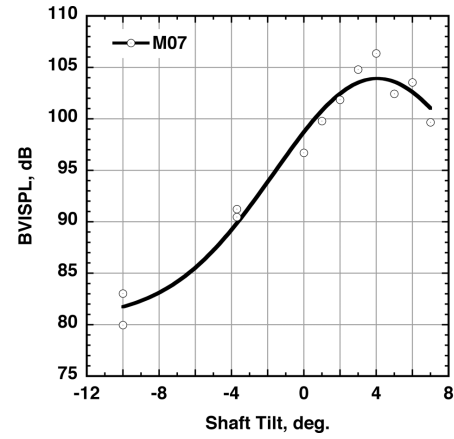


Figure 4. Baseline rotor BVISPL as a function of shaft tilt (positive aft) for Test Case 1 ($\mu = 0.150$, $\alpha = +4.0^\circ$) at microphone M07 (traverse station: -200)

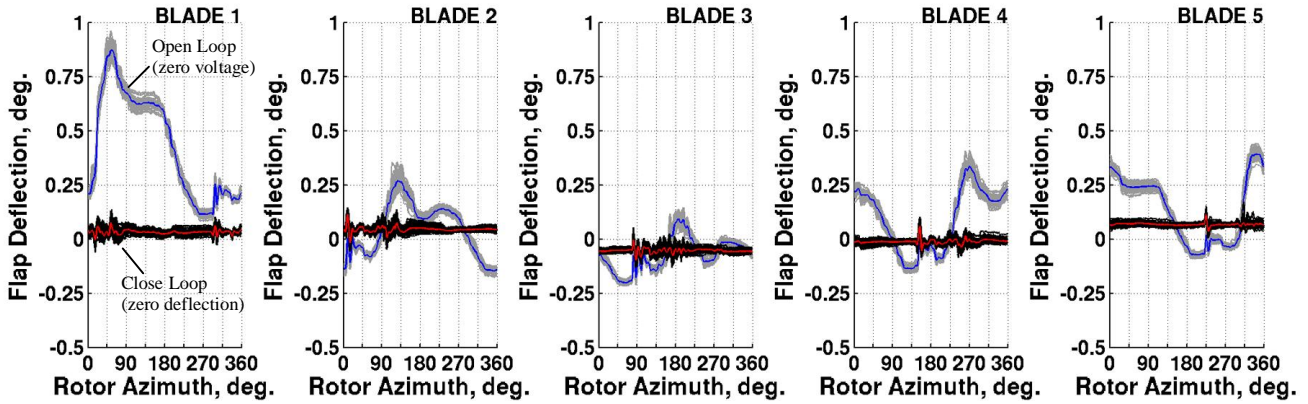


Figure 5. Flap deflection time histories for the baseline rotor (Test Case 1: $\mu = 0.150$, $\alpha = +4.0^\circ$); Blue line – open loop (zero voltage input) to all actuators, Red line – with closed-loop position control (zero deflection commanded).

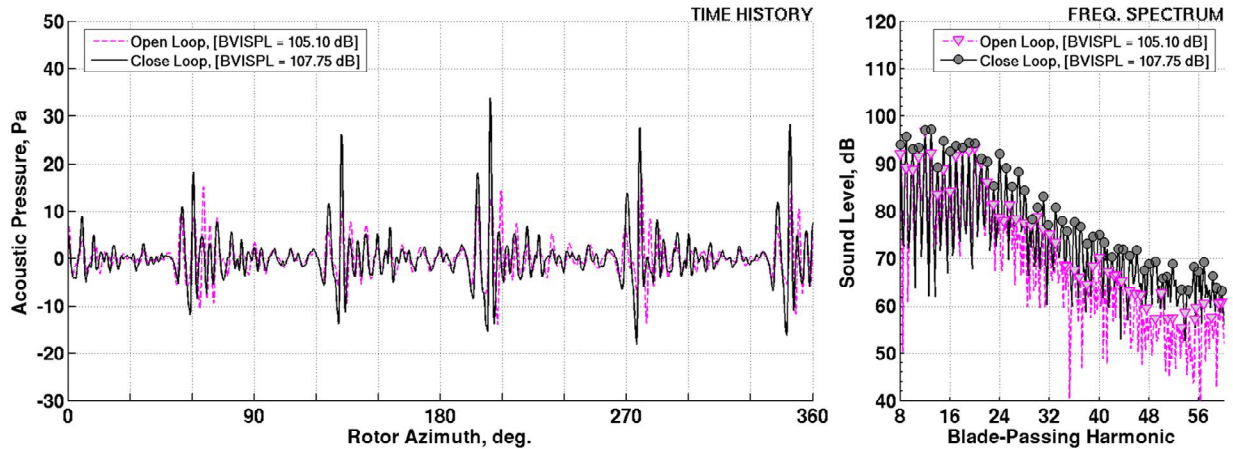


Figure 6. Acoustic time histories and spectral data comparisons for baseline rotor (Test Case 1: $\mu = 0.150$, $\alpha = +4.0^\circ$) at microphone M07 (traverse station: -200); solid gray line– open loop (zero voltage input) to actuators , pink dotted line- with closed-loop position control (zero deflection commanded).

During the course of the data acquisition, several data points were repeated to establish the fidelity and repeatability of noise measurement. As shown in Table 3, BVISPLs obtained for 12 repeated data points at microphone M07 (traverse station: -120 , $-.59R$) varied between 107.12 dB and 110.88 dB (with an average value of 109.75 dB and standard deviation of 1.27 dB). Adjacent microphones M08 and M09 also demonstrated similar trends showing BVISPL noise data to be repeated to within 4.5 dB. Note that the corresponding test conditions were replicated to within 1 to 2% variation in speed and thrust,

Prior to active flap excitations, a traverse sweep was also conducted to establish the spatial characteristics of baseline BVI noise radiation. Figure 7 shows two traverse plane carpet plots of measured BVISPLs for the baseline rotor for this test condition. On the left hand side is the carpet plot of un-averaged BVISPLs for one traverse sweep under the advancing disk; while on the right side is the carpet plot with BVISPLs obtained by averaging all available repeat points. In each plot, the traverse microphone locations are represented by white dots. At each traverse location (row of white dots), microphone M05 is on the left edge (cross-flow direction location of $0.41R$) and microphone M12 is on the right edge ($1.41R$) of the traverse plane. As noted earlier the traverse plane is $0.89R$ below the rotor center (at 0° shaft tilt) under the advancing rotor disk. There was only a slight difference between the noise levels between these two plots suggesting good noise data repeatability. For this test condition, a BVI hot spot was found slightly ahead of the rotor (between 0 and $-0.5R$) and on the advancing side of the rotor disk (between 0.41 to $0.75R$) where the averaged BVISPLs are 110 dB or higher. The strong forward and right side directivity is typical of BVI noise at this low speed. It should be noted that the distance between the rotor center and the microphone locations is not constant.

Table 3. Baseline Rotor Noise Data Repeatability
(Test Case 1: $\mu = 0.150$, $\alpha = +4.0^\circ$, traverse station: -120)

Repeat Data Point	MIC_07_ BVISPL, dB	MIC_08_ BVISPL, dB	MIC_09_ BVISPL, dB
1	111.54	111.22	110.40
2	108.71	107.92	106.70
3	107.12	106.77	105.96
4	110.09	109.46	108.18
5	108.15	107.61	106.34
6	110.49	109.58	107.86
7	110.52	110.69	110.02
8	110.51	109.86	108.63
9	110.88	110.51	109.38
10	110.17	109.66	108.39
11	108.91	108.46	106.73
12	109.87	108.88	107.20
Average	109.75	109.22	107.98
Standard Deviation	1.27	1.34	1.45

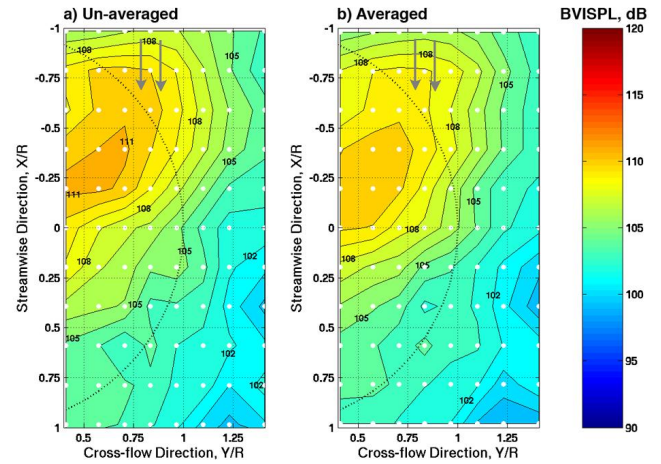


Figure 7. Measured baseline BVISPL contours for Test Case 1 ($\mu = 0.150$, $\alpha = +4.0^\circ$)

With the traverse parked at $-0.59R$ (traverse station -120), flaps were actuated at four different frequencies (2P, 3P, 4P and 5P) with varying input phase angles and amplitudes to determine the noise reduction potential of the single harmonic flap actuation. This microphone traverse position was selected based on the BVI hot spot (maximum BVISPL on the baseline rotor carpet plot) identified during the tests. As seen in Fig. 7, the hot spot is close to microphone M07 at this traverse position. Figure 8 shows the change in BVISPL from the average baseline value (109.75 dB) at microphone M07 as a function of harmonic frequency and phase input for flap amplitude of 1.5° . Noise reductions anywhere from 3 to 7 dB were found depending on the harmonic frequency and phase input. A flap amplitude sweep (from 1° to 2°) at 4P/30° was also conducted. It was determined that the active flap actuation at 4P with 1.5° amplitude and 30° phase amplitude provided best BVI noise level reduction at all microphone locations at this traverse location. Repeated data points with the same flap excitations also demonstrated good data repeatability that are consistent with findings reported in Table 3.

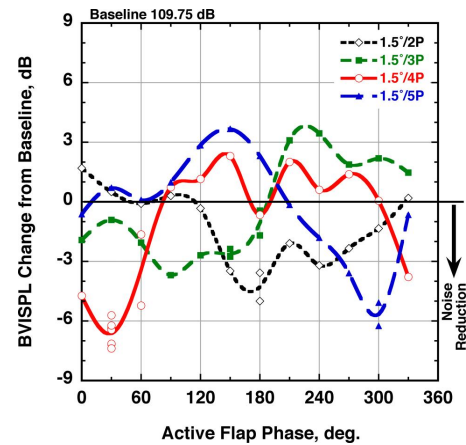


Figure 8. Effect of active flap excitation on BVISPL for Test Case 1 ($\mu = 0.150$, $\alpha = +4.0^\circ$) at microphone M07 (traverse station: -120)

A traverse sweep was conducted with the $1.5^\circ/4P/30^\circ$ flap actuation. Figure 9 shows the carpet plots of BVISPL contours for the baseline rotor, rotor with $1.5^\circ/4P/30^\circ$ flap actuation and the difference (active flap rotor noise levels minus the baseline rotor noise levels) in noise levels between the two. BVISPL values used in these contours are averaged over repeat data points where available. Figure 9 clearly shows that the active flap was able to reduce the BVI noise over a wide range of directivity angles under the advancing disk with BVISPL reductions as high as 7 dB under advancing side of rotor disk. With active flap, the BVISPLs at the baseline hot spot location was reduced by as much as 3.5 to 6 dB. Figure 10 shows the time history and spectral data comparisons between the baseline rotor and the rotor

with $1.5^\circ/4P/30^\circ$ flap actuation for microphone M07 with traverse at $-0.59R$. Figure 10 clearly shows the reduced acoustic pressure and higher harmonic spectral levels with flap actuation resulting in 7.1 dB reduction in BVISPL relative to the baseline demonstrating the effectiveness of harmonic flap actuation for reducing BVI noise. However, this active flap actuation which produced large BVI noise reductions also produced large increases in vibratory hub loads relative to those for the baseline rotor as shown in Fig. 11. This trend was also observed for other actively controlled (HHC and Root pitch IBC) rotors [7, 10].

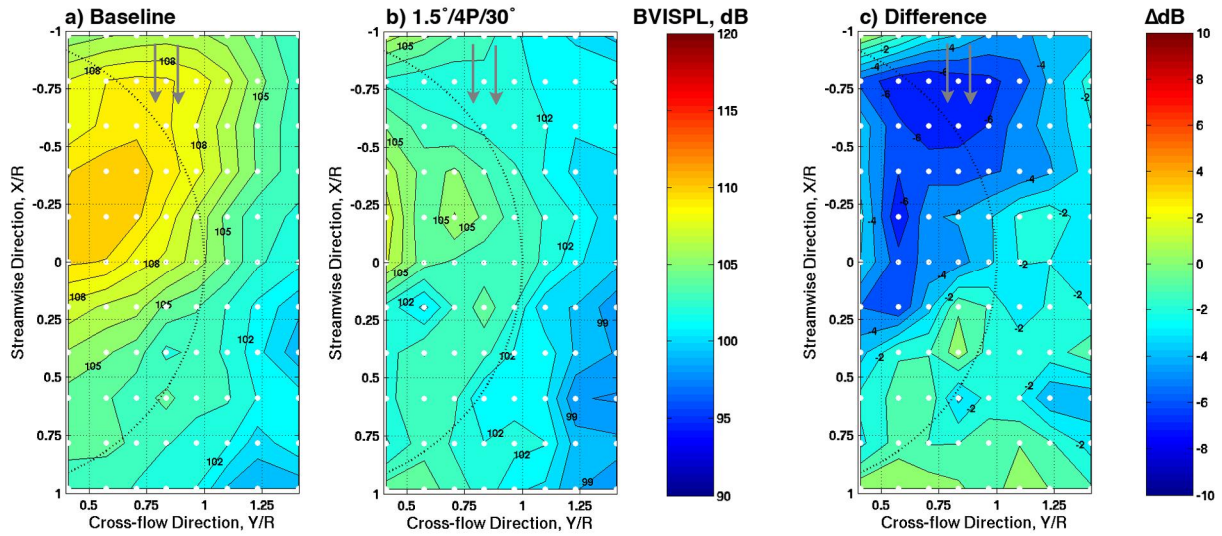


Figure 9. BVISPL contours for baseline and active flap actuation ($1.5^\circ/4P/30^\circ$) for Test Case 1 ($\mu = 0.150$, $\alpha = +4.0^\circ$)

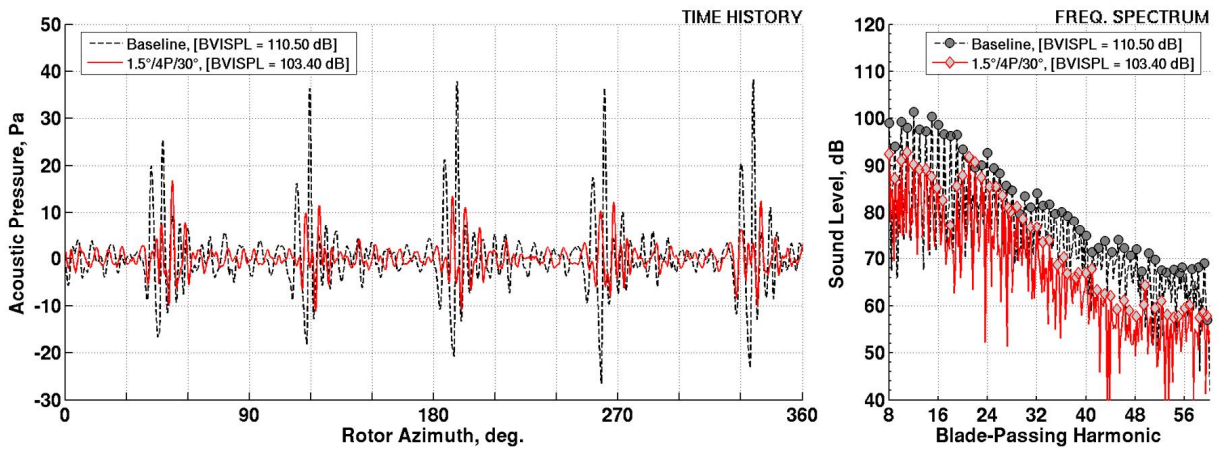


Figure 10. Acoustic pressure time histories and spectral data for baseline and active flap actuation ($1.5^\circ/4P/30^\circ$) for Test Case 1 ($\mu = 0.150$, $\alpha = +4.0^\circ$) at microphone M07 (traverse station: -120 , $-.59R$)

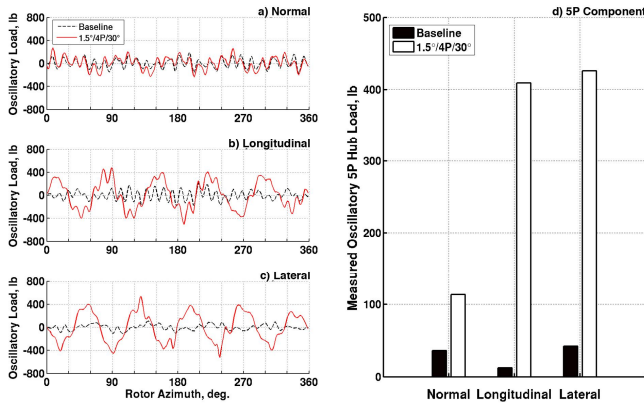


Figure 11. Vibratory hub loads for baseline and active flap actuation ($1.5^\circ/4P/30^\circ$) for Test Case 1 ($\mu = 0.150$, $\alpha = +4.0^\circ$)

As discussed earlier, BVI rotor noise predictions were made using CAMRAD II and PSU-WOPWOP codes. Figure 12 shows the predictions for the baseline rotor and the active flap rotor with $1.5^\circ/4P/30^\circ$ flap actuation. A comparison with measured data (see Fig.9) shows that for the baseline rotor the maximum predicted noise levels are comparable to the measured data and the directivity is not well captured. The predicted BVI hot spot was more downstream compared to the test data. For the active flap rotor with $1.5^\circ/4P/30^\circ$ flap actuation, predictions, unlike test data showed a slight increase in BVISPLs. Predictions were then made for several input phase angles at $1.5^\circ/4P$. A phase input angle of 180° was found to be effective in reducing the BVISPLs over a large range of directivity angles underneath the advancing side (Fig. 13). Unlike in test data, large BVISPL reductions of the order of 6 dB were found downstream underneath the advancing rotor disk.

Predictions were also made over a much larger plane underneath the rotor to investigate the effectiveness of the active flap rotor at locations under the rotor where test data could not be obtained such as those on the retreating side and further upstream. Figure 14 shows that for the best phase setting of 180° , BVISPL reductions on the retreating side were small and there were slight BVISPL increases at locations further upstream. However, the active flap was found to be very effective in reducing BVI noise over a wide range of directivity angles including those downstream. While the predictions showed that the active flap is indeed very effective in reducing the BVI noise, the predictions (especially the input phase angle) did not correlate with test data. It is believed that more advanced CFD (Computational Fluid Dynamics) methods coupled to CAMRAD II, similar to the ones developed in recent years to model successfully the active root pitch control rotors [38-40], may be needed to accurately model the active flap rotors.

Test Case 2: $\mu = 0.165$, $C_T/\sigma = 0.075$, $M_{tip} = 0.617$

As noted earlier, this test case was specifically chosen to simulate the MD 902 helicopter FAA noise certification approach test condition of 68 knots and 6° glide-slope. The shaft tilt was estimated to be 1.8° aft. For the baseline rotor (0° flap deflection with closed-loop position control), a traverse sweep was conducted to generate BVISPL carpet plot and identify the BVI hot spot. The BVI hot spot (maximum BVISPL) was found near microphone M06 at traverse station of -80 ($-0.39R$). The noise data repeatability was also found to be good for this test condition.

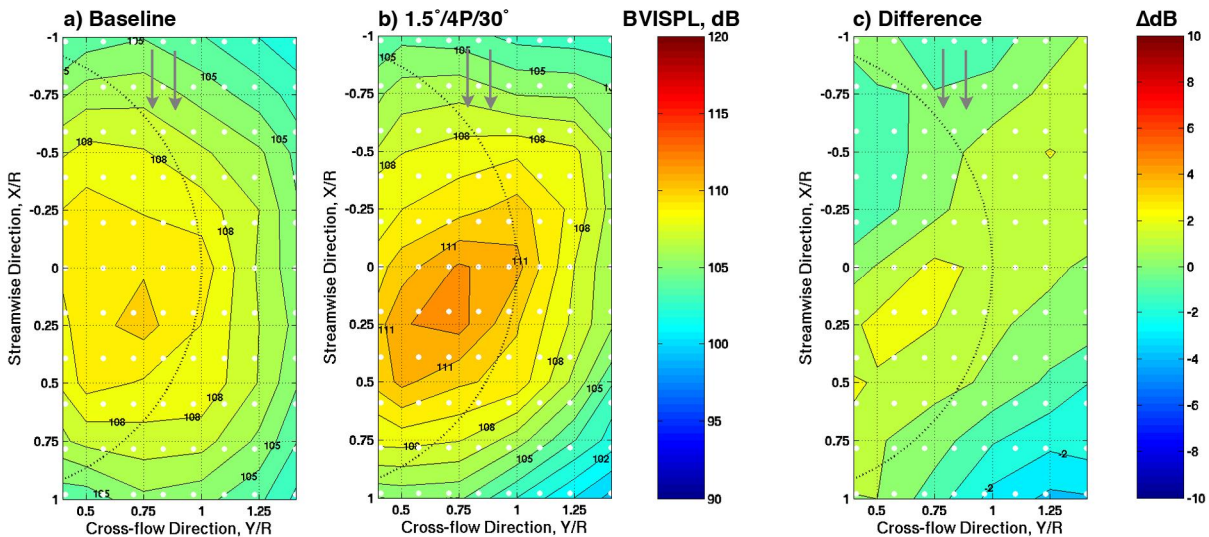


Figure 12. CAMRAD II/PSU-WOPWOP predictions for baseline and active flap actuation ($1.5^\circ/4P/30^\circ$): Test Case 1 ($\mu = 0.150$, $\alpha = +4.0^\circ$)

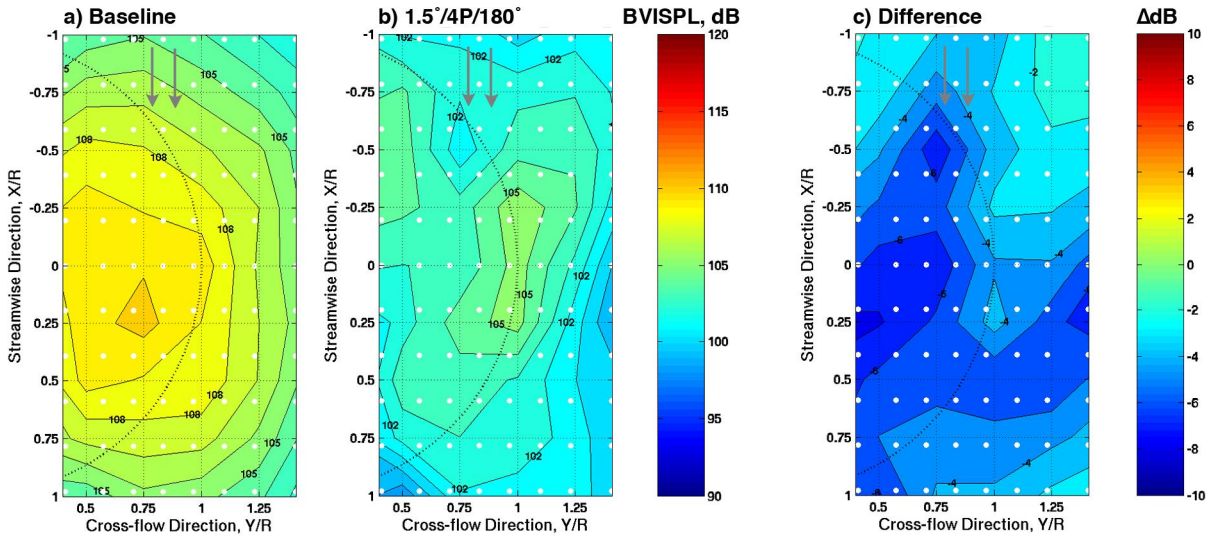


Figure 13. CAMRAD II/PSU-WOPWOP predictions for baseline and active flap actuation ($1.5^\circ/4P/180^\circ$): Test Case 1 ($\mu = 0.150$, $\alpha = +4.0^\circ$)

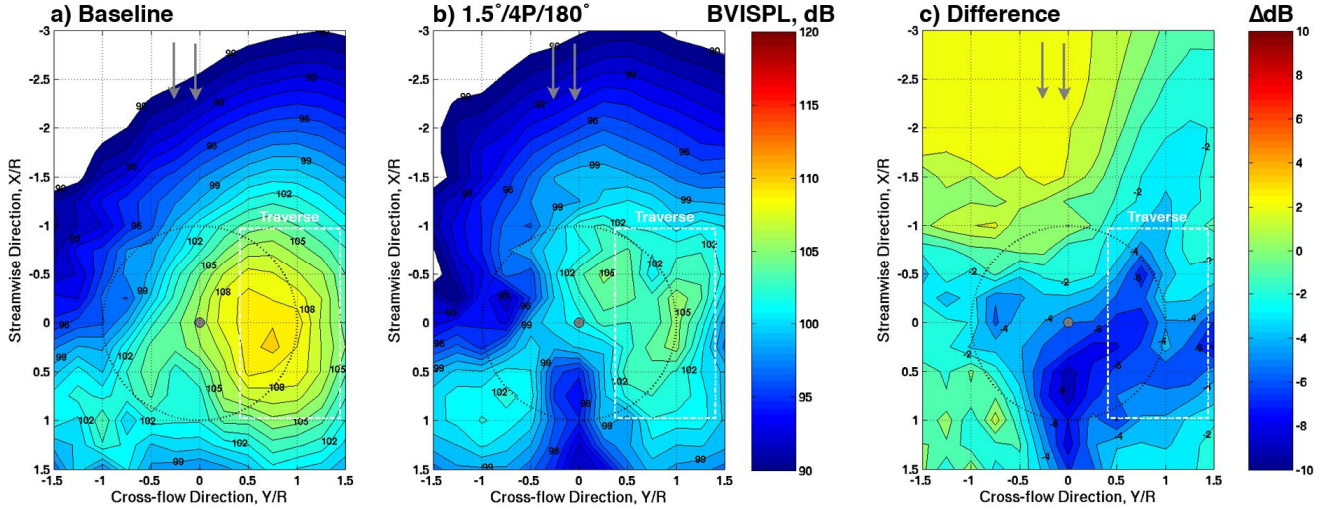


Figure 14. CAMRAD II/PSU-WOPWOP predictions for locations on a large plane under the rotor for baseline and active flap actuation ($1.5^\circ/4P/180^\circ$): Test Case 1 ($\mu = 0.150$, $\alpha = +4.0^\circ$)

With the traverse parked at station -80 (-.39R), flaps were actuated at two different frequencies (3P and 4P) with varying input phase angles and amplitudes to determine the noise reduction potential of the flap actuation. Figure 15 shows the variation of change in BVISPL from the average baseline value (107.23 dB) at microphone M06 with harmonic frequency and phase input for flap amplitude of 1.5° . Noise reductions anywhere from 4.5 to 6 dB were found depending on the harmonic frequency and phase input. Although some data variability was found later at phase 180° for 3P (Fig. 15), $3P/180^\circ$ with 1.5° amplitude was chosen during the tests as the combination of active flap parameters which will produce the highest BVI noise reduction. A traverse sweep was conducted with the $1.5^\circ/3P/180^\circ$ flap actuation. Figure 16 shows the traverse

plane carpet plots of BVISPL contours for the baseline rotor, rotor with $1.5^\circ/3P/180^\circ$ flap actuation and the difference in noise levels between the active flap on and baseline. BVISPL values used in these contours are averaged over repeat data points where available. Figure 16 clearly shows that the active flap was able to reduce the BVI noise over a wide range of directivity angles under the advancing disk with BVISPL reductions of 4 to 5 dB or more near the upstream locations under advancing side of rotor disk. With active flap, the BVISPLs at the baseline hot spot locations were reduced by as much as 3 to 5 dB. The BVISPL noise reductions with active flap were found to be comparable, but slightly lower than those observed for the lower speed flight condition corresponding to Test Case 1 ($\mu = 0.150$, $\alpha = +4.0^\circ$).

As was the case with the lower speed test, this active flap actuation also produced large increases in vibratory hub loads relative to those for the baseline rotor as shown in Fig.17 although the increases in hub loads are not as large as those seen for the lower flight speed. Noise predictions for both baseline and active flap rotors were made with CAMRAD II/PSU-WOPWOP codes (Figs. 18 and 19). A comparison between test data and predictions for the baseline rotor (Figs. 16 and 18) shows that the predicted BVISPLs are within 1 or 2 dB from measurements and the predicted BVI hot spot location is more downstream. The measured BVISPL noise reductions for active flap actuation $1.5^\circ/3P/180^\circ$ were not predicted (Fig. 18). In fact for this flap actuation, predictions showed slight BVISPL increases at several microphone locations on the traverse plane. However, as shown in Figure 19 flap actuation with 270°

phase angle ($1.5^\circ/3P/270^\circ$), active flap did reduce BVISPLs at the traverse plane. These prediction trends are similar to the ones observed for the previous case.

Test Case 3: $\mu = 0.200$, $C_T/\sigma = 0.075$, $M_{tip} = 0.623$

As noted earlier, this case was tested to establish BVI noise characteristics of the active flap rotor at a relatively high speed. Similar procedures as were used for test case 1 showed that a shaft tilt of 2° aft produced the most BVI noise at the traverse plane. At this shaft tilt setting, a traverse sweep was conducted for the baseline rotor (0° flap deflection with closed-loop position control). The noise data repeatability was also found to be good for this test condition.

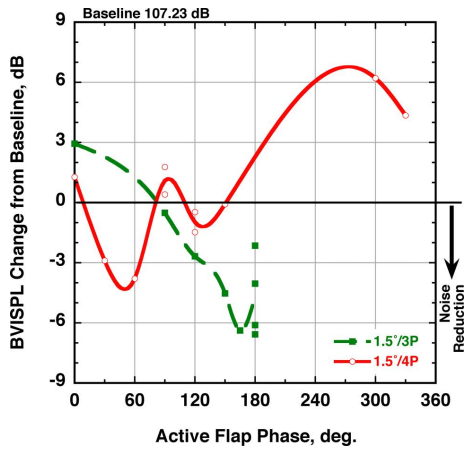


Figure 15. Effect of active flap excitation on BVISPL for Test Case 2 ($\mu = 0.165$, $\alpha = +1.8^\circ$) at microphone M06 (traverse station: -80)

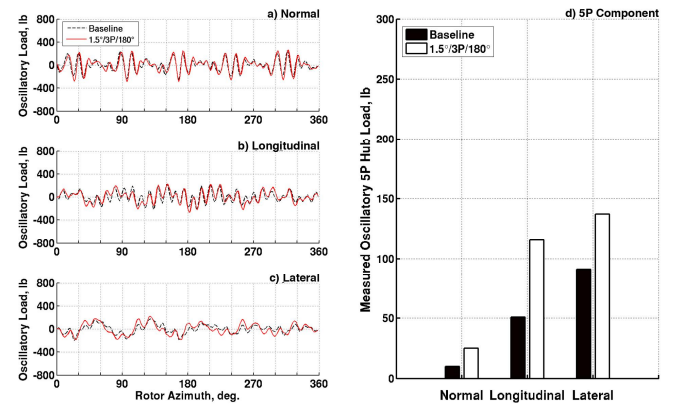


Figure 17. Vibratory hub loads for baseline and active flap actuation ($1.5^\circ/3P/180^\circ$) for Test Case 2 ($\mu = 0.165$, $\alpha = +1.8^\circ$)

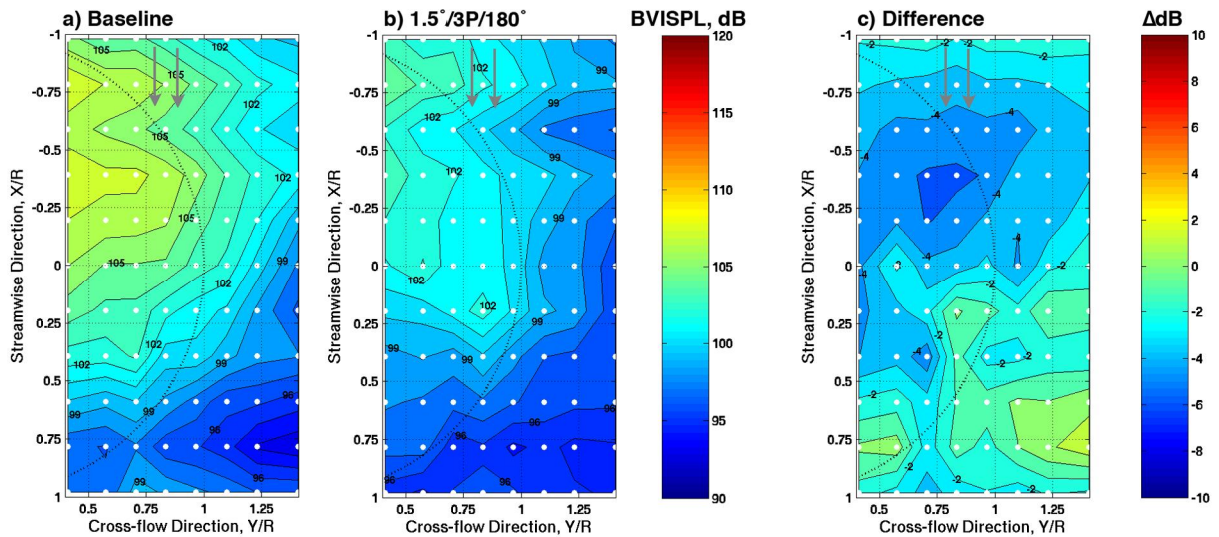


Figure 16. BVISPL contours for baseline and active flap actuation ($1.5^\circ/3P/180^\circ$) for Test Case 2 ($\mu = 0.165$, $\alpha = +1.8^\circ$)

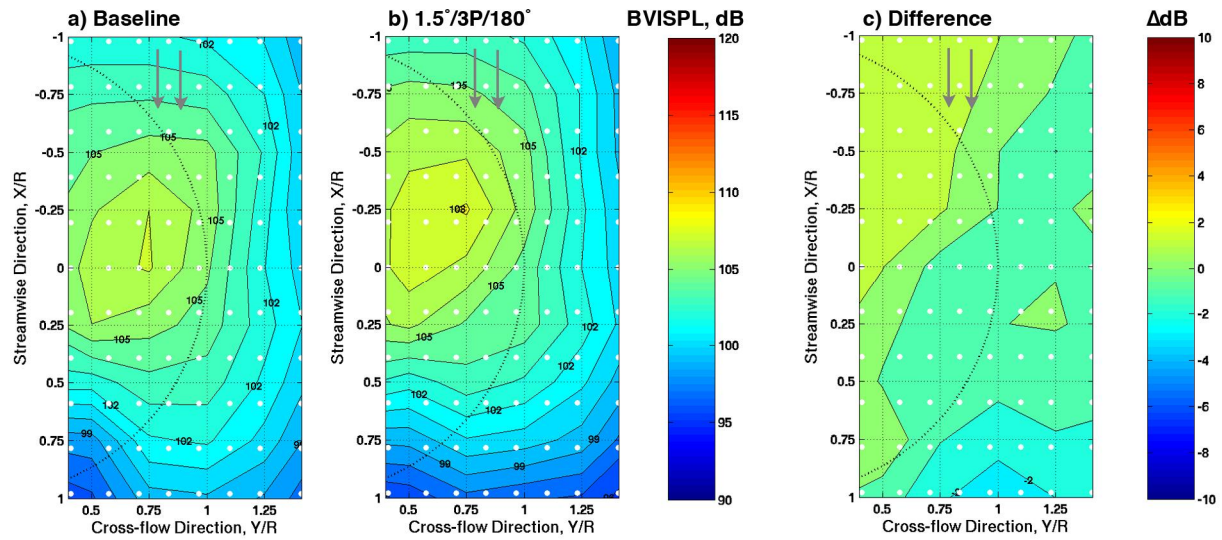


Figure 18. CAMRAD II/PSU-WOPWOP predictions for baseline and active flap actuation ($1.5^\circ/3P/180^\circ$): Test Case 2 ($\mu = 0.165$, $\alpha = +1.8^\circ$)

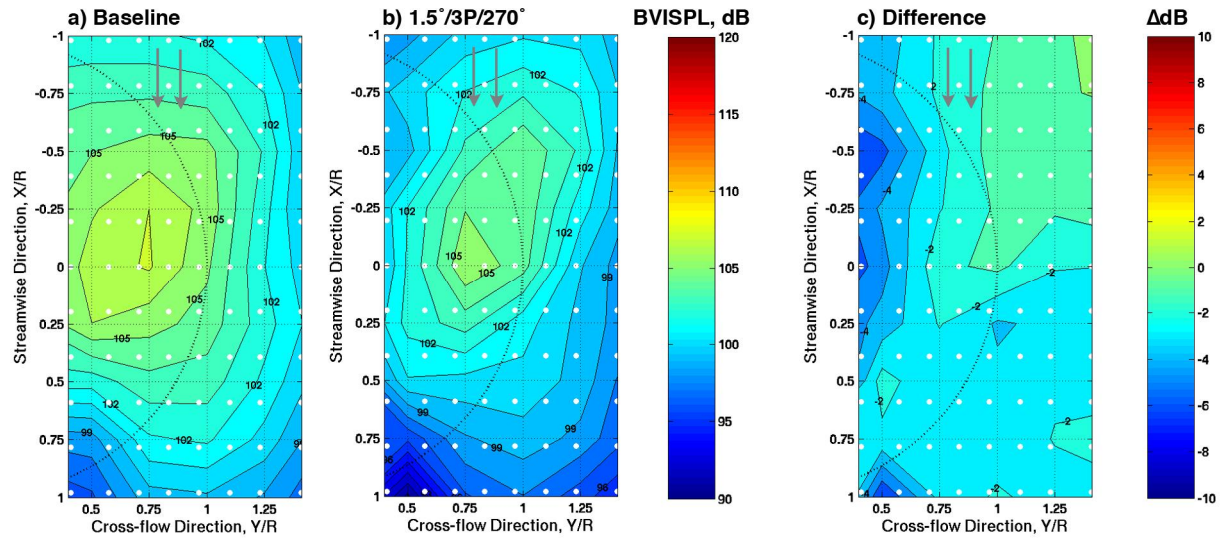


Figure 19. CAMRAD II/PSU-WOPWOP predictions for baseline and active flap actuation ($1.5^\circ/3P/270^\circ$): Test Case 2 ($\mu = 0.165$, $\alpha = +1.8^\circ$)

Measured BVISPLs on the traverse plane showed that the BVI hot spot is near microphone M09 at a traverse station of -40. With the traverse parked at this position, flaps were actuated at four different frequencies (2P, 3P, 4P and 5P) with varying input phase angles and amplitudes to determine the noise reduction potential of the flap actuation. Figure 20 shows the variation of change in BVISPL from the average baseline value (110.43 dB) at microphone M09 (traverse station: -40, -2R) as a function of harmonic frequency and phase input for flap amplitude of 1.5° . Noise reductions anywhere from 1 to 3.5 dB were found. Although some data variability was discovered later (Fig. 20), 3P/180° with 1.5° amplitude was chosen as the “best” active flap excitation that offered the most BVI noise reduction.

A traverse sweep was conducted with the $1.5^\circ/3P/180^\circ$ flap actuation. Figure 21 shows the traverse plane carpet plots of BVISPL contours for the baseline rotor, rotor with $1.5^\circ/3P/180^\circ$ flap actuation and the difference in noise levels between the two. BVISPL values used in these contours are averaged over repeat data points where available. Figure 21 shows that the BVI noise reductions with this active flap actuation were not as high (often less than 3 dB) as those found at lower flight speeds (test cases 1 and 2). In fact at several traverse plane microphone locations, the BVISPLs increased slightly (1 to 2 dB) with this flap actuation. It is quite possible that other flap actuation settings identified in phase sweeps (Fig. 20) such as 2P/30° with 2° flap amplitude could have produced higher BVI noise reductions over the traverse plane.

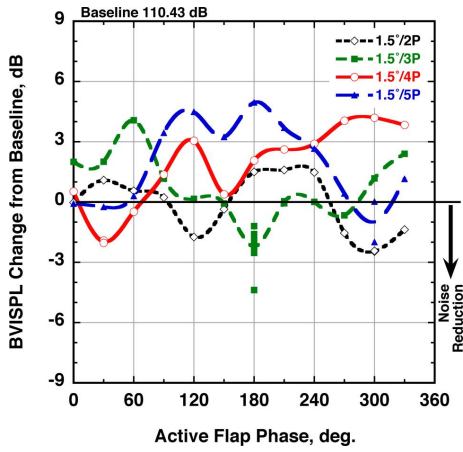


Figure 20. Effect of active flap excitation on BVISPL for Test Case 3 ($\mu = 0.200$, $\alpha = +2.0^\circ$) at microphone M09 (traverse station: -40)

As expected, the $1.5^\circ/3P/180^\circ$ flap actuation did increase the hub loads (Fig. 22) although there was a slight decrease in normal (vertical) hub load with active flap. Predictions made with CAMRAD II/PSU-WOPWOP showed much higher noise levels for the baseline rotor (Fig. 23) at the traverse plane compared to those measured (Fig. 21) and the predicted BVI hot spot covered a much wider region. Predictions also showed that active flap with the $1.5^\circ/3P/180^\circ$ actuation increased the BVISPLs over the traverse plane. However, with a 330° phase setting at 3P and 1.5° flap amplitude, BVISPL reductions of 1 to 2 dB were predicted (Fig. 24) at most of the traverse plane locations.

LIMITATIONS & ISSUES

Although it was shown that active flap can be very effective in reducing BVI noise, a clear understanding of why certain harmonics and phase settings identified

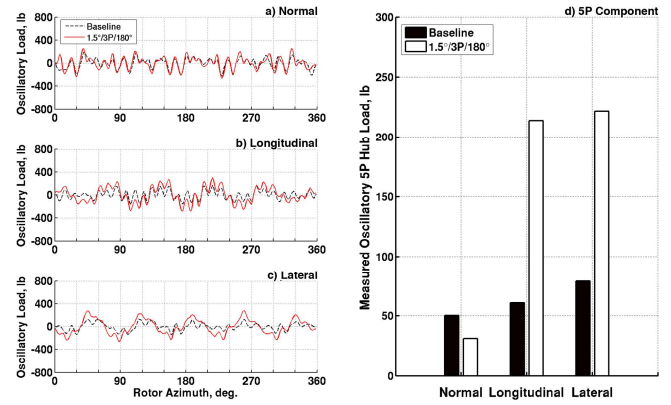


Figure 22. Vibratory hub loads for baseline and active flap actuation ($1.5^\circ/3P/180^\circ$) for Test Case 3 ($\mu = 0.200$, $\alpha = +2.0^\circ$)

during the tests for BVI noise reduction were effective was not established. It is well known that BVI noise reduction can be achieved through blade airload modifications at certain azimuths. Here active flaps through indirect lift control (servo effect, Ref. 27) may have modified airloads such that, with the identified active flap settings identified for BVI noise reduction, blades may have generated weaker tip vortices in the second rotor quadrant and the resulting downwash field may have pushed these vortices away from the blades in the blade-vortex interaction region (usually in the first quadrant for strong BVI) and thus increase the miss distance. These active flap settings may also have changed the blade flapping such that the miss distance is increased. A detailed set of wake and airloads measurements would have uncovered the reasons behind the observed BVI noise reductions.

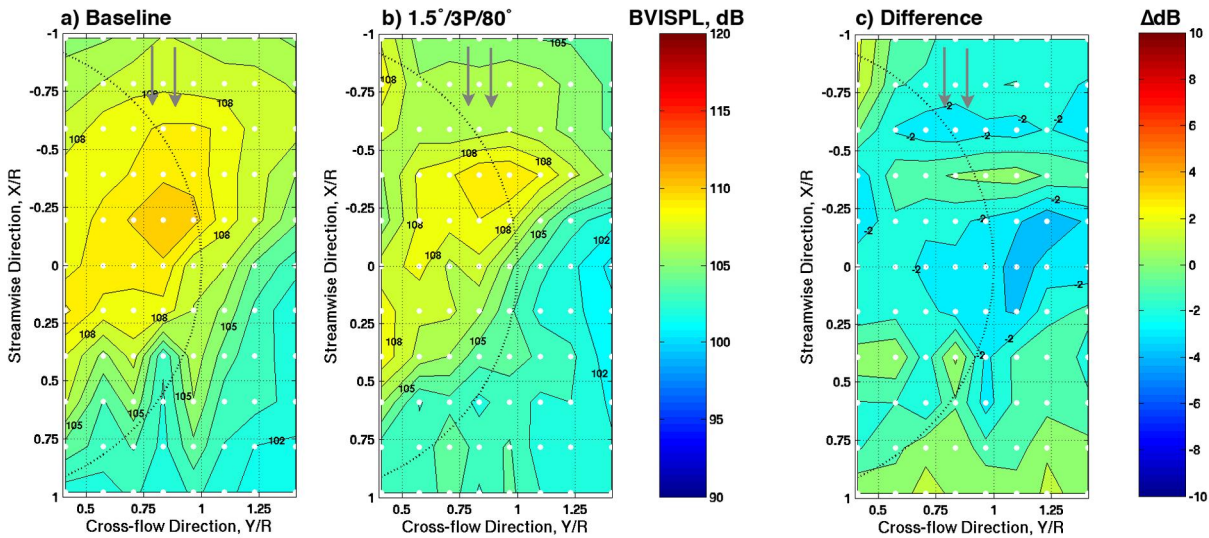


Figure 21. BVISPL contours for baseline and active flap actuation ($1.5^\circ/3P/180^\circ$) for Test Case 3 ($\mu = 0.200$, $\alpha = +2.0^\circ$)

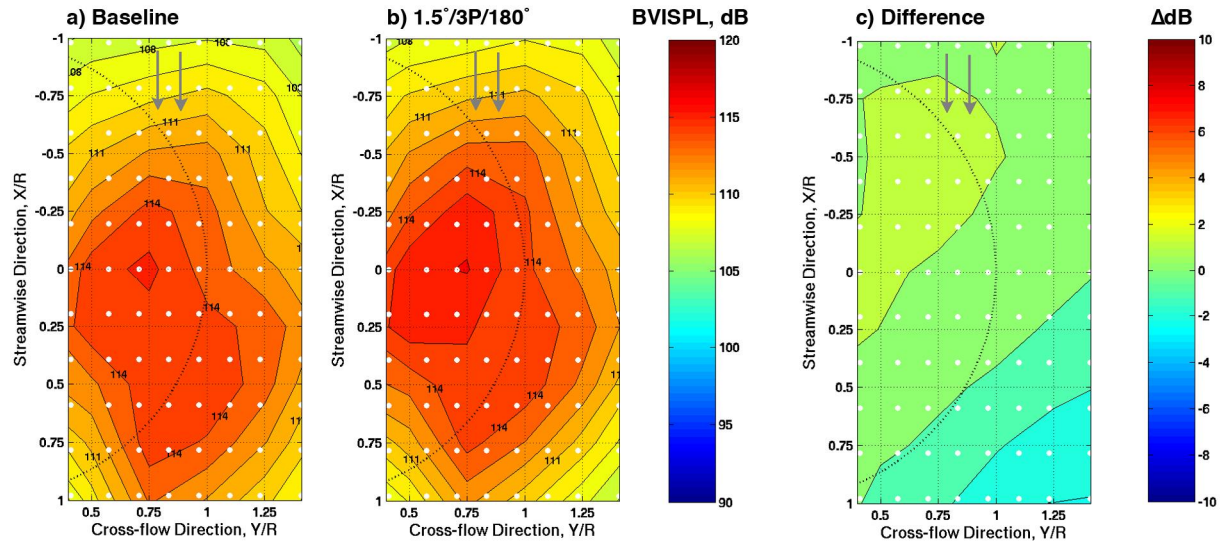


Figure 23. CAMRAD II/PSU-WOPWOP predictions for baseline and active flap actuation (1.5°/3P/180°):
Test Case 3 ($\mu = 0.200$, $\alpha = +2.0^\circ$)

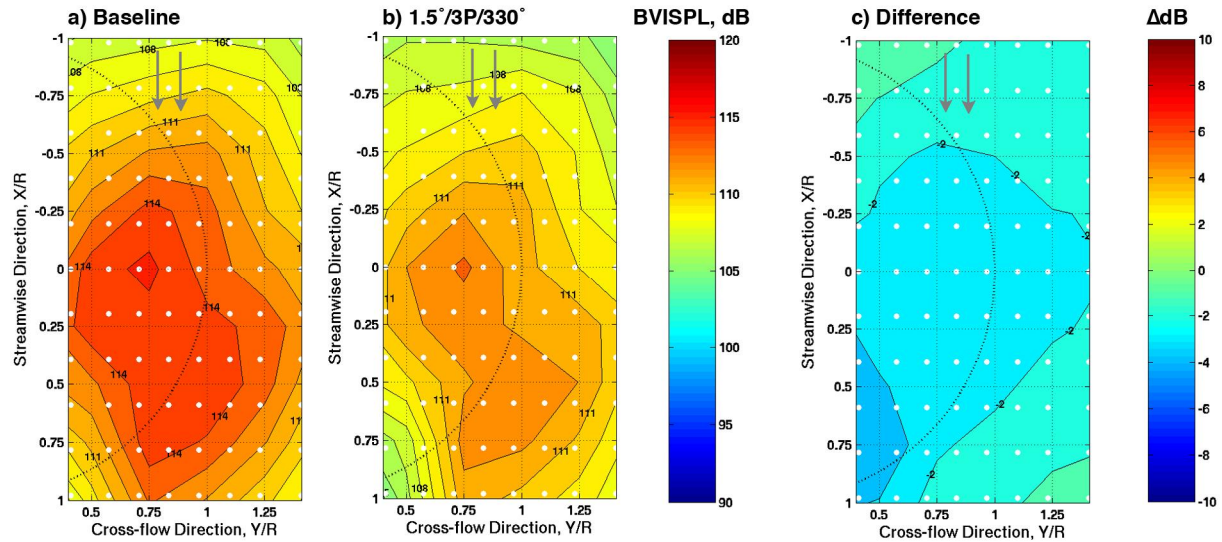


Figure 24. CAMRAD II/PSU-WOPWOP predictions for baseline and active flap actuation (1.5°/3P/330°):
Test Case 3 ($\mu = 0.200$, $\alpha = +2.0^\circ$)

In the absence of such detailed measurements, a well – correlated prediction code (with this test data) could have been used to explain the mechanisms associated with BVI noise reductions due to active flaps. The CAMRAD II/PSU-WOPWOP predictions did not correlate well with the test data especially the phase settings for BVI noise reductions. It is believed that more advanced coupled CFD and CSD (computational structural dynamics) prediction codes are needed to model active flap rotors.

Another limitation of the tests was that the test set-up did not allow for microphones on either the retreating side of the disk or a larger traverse plane underneath the rotor.

While the active flap was able to reduce the BVI noise on the traverse plane used, it is not known how effective the active flap is in reducing the BVI noise at other locations especially on the retreating side and those ahead of and closer to the rotor center line. Again, a prediction code well – correlated with this test data would have been able to address these issues. Also, only single harmonic excitations were used during these tests. Neither closed-loop control of active flap for BVI noise reduction nor open-loop mixed harmonic excitation of the active flap could be performed during these tests. The latter could have been more effective in reducing BVI noise by a larger margin and/or over a larger area underneath the rotor.

In addition, the use of active flap to reduce mid-to-high frequency BVI noise causes some increase in noise in the lower frequencies. As shown in Fig. 25 for the BVI hot spot (microphone M07, traverse station -120) for test case 1, actuating the flap at $1.5^\circ/4P/30^\circ$ can amplify (not uniformly) the harmonic content in the first through the seventh blade passage frequency by up to 8 dB compared to baseline. This effect has been observed in other active control tests as well [14], but is deemed not of concern for community annoyance assessment due to the insensitivity of human hearing at these low frequencies. This is reflected by the A-weighted sound pressure level metric (AWTSPL) illustrated in Fig. 25.

Another area of concern is the increase in vibratory rotor hub loads typically incurred by the use of active controls to reduce noise. For the Boeing-SMART Rotor,

although the reported amplification in vibratory hub loads (from baseline) is disconcerting, the net increase is deemed not a limiting factor for safety, life-cycle fatigue and cabin comfort considerations. Figure 26 shows that vibratory hub loads resulting from active flap excitations during low speed, low BVI noise operations discussed in this paper, are comparable to a nominal higher airspeed condition. With the exception of the lateral component for test case 1, all measured vibratory hub load components are of the same order of magnitude, or lower, compared to baseline, level-flight condition corresponding to 155 kts ($\mu = 0.375$, $\alpha = -9.3^\circ$, $C_T/\sigma = 0.065$, $M_{tip} = 0.620$). Therefore, the incurred hub load penalties are likely to be an acceptable “ride-quality” trade-off for low noise terminal operations. It is also believed that some of the hub load issues can be alleviated via mixed harmonic excitations of the active flap to simultaneously reduce noise and vibratory hub loads.

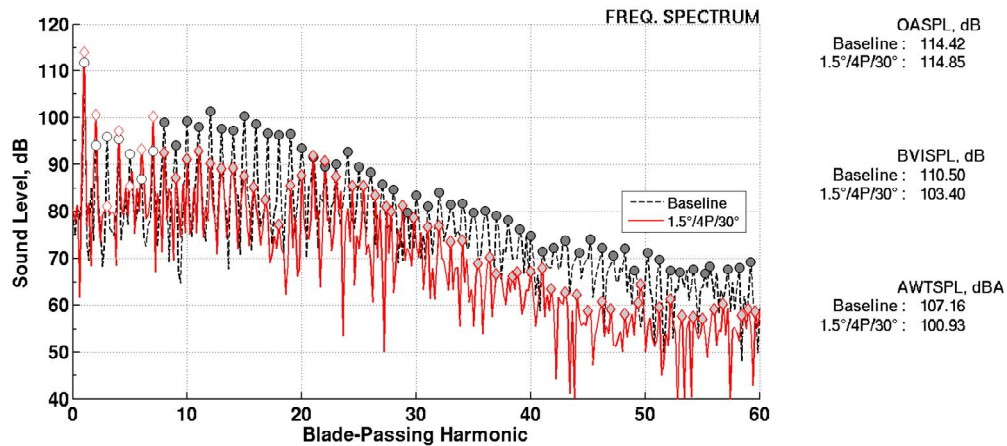


Figure 25. Spectral data for baseline and active flap actuation ($1.5/4P/30^\circ$) for Test Case 1 ($\mu = 0.150$, $\alpha = +4.0^\circ$) at microphone M07 (traverse station: -120)

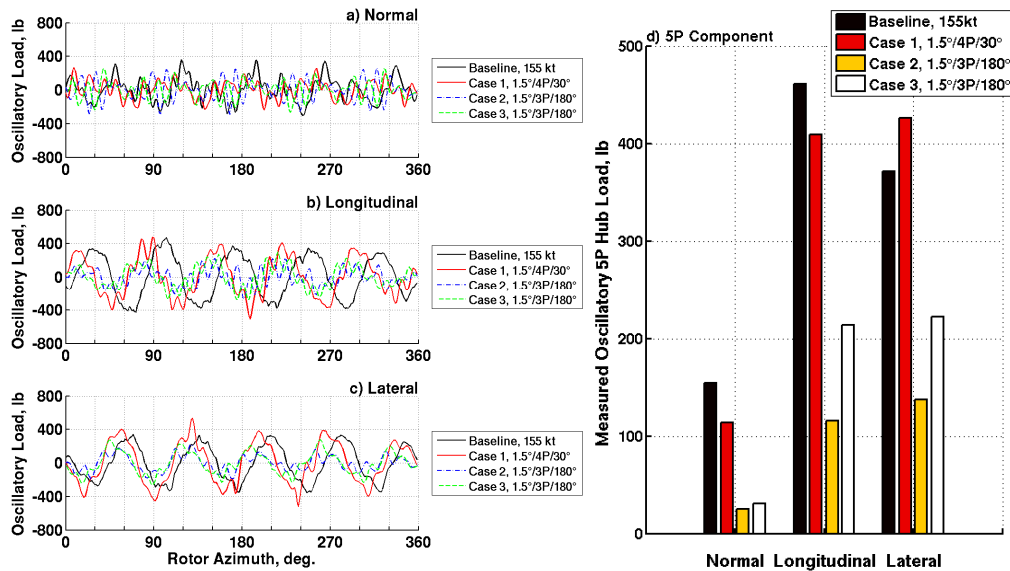


Figure 26. Comparisons of measured hub loads of active flap actuation (Test Cases 1 to 3) with baseline 155 kts (level-flight) condition

CONCLUSIONS

Acoustic measurements of a full-scale active flap rotor obtained from the joint Boeing/DARPA/NASA/Army test in the Air Force National Full-Scale Aerodynamic Complex's 40- by 80-foot anechoic wind tunnel demonstrated the potential of active flaps to reduce BVI noise over a wide range of directivity angles underneath the advancing rotor disk. Results are shown for three simulated descent flight conditions where BVI noise radiation was expected to be dominant for the baseline rotor. The baseline rotor for each test condition was simulated with 0° flap deflections (achieved via closed loop flap position flap control) on all the blades. For each test condition, open-loop single harmonic flap excitations with varying frequencies (2- to 5-per-rev), input phase and amplitude were used to demonstrate BVI noise reductions. Active flap schedules (certain combinations of flap frequency, amplitude and phase) were identified which showed BVI noise reductions from 2 to 7 dB depending on the flight speed. Predictions made with CAMRAD II/PSU-WOPWOP code did not correlate well with active flap test data although the noise levels for baseline rotor were predicted reasonably well for low speed cases. BVI noise was quantified in terms of BVISPL metric which is a summation of spectral levels between 8th and 60th blade passage frequency. The following specific conclusions were reached.

- 1) The noise data repeatability for the baseline rotor has been good. Standard deviations from the average of the BVISPLs are on the order of 1.5 dB. With active flap actuation, the variation is slightly higher.
- 2) For a low speed test case ($\mu = 0.150$), a shaft angle of 4° aft generated the highest BVI noise levels underneath the advancing rotor disk. With an active flap schedule of 1.5°/4P/30° (flap amplitude of 1.5° with 4 per rev frequency and 30° phase), BVISPL reductions of up to 7 dB were measured under advancing side of rotor disk. At the baseline rotor BVI hot spot location, BVISPL reductions varied between 3.5 and 6 dB.
- 3) For the simulated FAA noise certification approach flight condition for an MD 902 helicopter ($\mu = 0.165$, and a shaft angle of 1.8° aft), an active flap schedule of 1.5°/3P/180° was able to reduce BVI noise levels by as much as 5 dB. Noise reductions at the baseline rotor BVI hot spot locations varied between 3 and 5 dB.
- 4) For the moderate high speed test case ($\mu = 0.200$), a shaft angle of 2° aft generated the highest BVI noise levels under the advancing rotor disk. With an active flap schedule of 1.5°/3P/180°, relatively small BVISPL reductions (a maximum of about 3 dB) were measured under the rotor disk.
- 5) Noise predictions made with the comprehensive aeroelastic analysis code CAMRAD II and acoustic prediction code PSU-WOPWOP were reasonably well correlated with the baseline rotor (no active flap) test data for the two low speed test cases although the predicted BVI hot spot location was more downstream compared to the test data. For the high speed case ($\mu = 0.200$), the BVI noise levels for the baseline rotor were over-predicted by at least 3 dB. The correlation between predicted noise levels and test data for the active flap schedules used has been poor. In particular, active flap phase for minimum BVI noise was not well predicted. However, for all the three test cases, at different phase settings, predictions showed BVI noise reductions with active flaps with the largest reductions (up to 6 dB) predicted for the low speed test case ($\mu = 0.150$).
- 6) Vibratory hub loads (normal, lateral and longitudinal) increased for flap schedules used for BVI noise reduction.

ACKNOWLEDGMENTS

Funding for the wind tunnel test was provided by DARPA as part of the Helicopter Quieting Program and by the NASA Subsonic Rotary-Wing program. The authors wish to thanks Dr. Wayne Johnson for his CAMRAD II airloads predictions. The valuable contributions of the many dedicated staff members at Boeing, NASA, Army, MIT, UCLA, and University of Maryland are gratefully acknowledged.

REFERENCES

1. JanakiRam, R. D., "Aeroacoustics of Rotorcraft", AGARD Report No. 781, Aerodynamics of Rotorcraft, November 1990.
2. Yu, Y. H., "Rotor blade-vortex interaction noise", Progress in Aerospace Sciences, Vol. 36, (2), February 2000, pp. 97-115.
3. Schmitz, F. H. and Sim, B. W., "Radiation and Directionality Characteristics of Helicopter Blade-Vortex Interaction Noise", Journal of the American Helicopter Society, Vol. 48, (4), October 2003, pp. 253-269.
4. Brooks, T. F., "Studies of Blade-Vortex Interaction Noise by Rotor Blade Modifications", Proceedings of the 1993 National Conference on Noise Control, Williamsburg, VA, 199, pp 57-66.
5. Nakamura, H., Nishimura, H., Kondo N., Yamakawa, E., Ayoma, T. and Saito, S., "Effect of Blade Geometry on BVI Noise in Various Flight Conditions", Heli Japan 98, Gifu, Japan, 1998.
6. Bebesel, M., Ploz, G. and Schoell, E., Aerodynamic and Aeroacoustic Layout of the ATR (Advanced Technology Rotor)", Proceedings of the 55th Annual Forum of the American Helicopter Society, Montreal, Canada, May 25-27, 1999.
7. Splettstoesser, W. R., Schultz, K. J., Kube, R., Brooks, T. F., Booth, E. R., Niesl, G. and Streby, O., "A Higher Harmonic Control Test in the DNW to Reduce Impulsive BVI Noise", Journal of the American Helicopter Society, Vol. 39, (4).
8. Yu, Y. H., Gmelin, B., Splettstoesser, W. R., Philippe, J. J., Prieur, J. and Brooks, T. F., "Reduction of Helicopter Blade-Vortex Interaction Noise by Active Rotor Control

- Technology", Progress in Aerospace Sciences, Vol. 33, Issues 9-10, 1997, pp. 647-687.
9. Yu, Y. H., Tung, C., van der Wall, B. G., Pausder, H., Burley, C., Brooks, T., Beaumier, P., Delrieux, Y., Mercker, E. and Pengel, K., "The HART II Test: Rotor Wakes and Aeroacoustics with Higher-Harmonic Pitch Control (HHC) Inputs – The Joint German/French/Dutch/US Project", Proceedings of the 58th Annual Forum of the American Helicopter Society, Montreal, Canada, June 11-13, 2002.
 10. Jacklin, S. A., Blaas, A., Teves, D. and Kube, R., "Reduction of Helicopter BVI Noise, Vibration and Power Consumption Through Individual Blade Control", Proceedings of the 51st Annual Forum of the American Helicopter Society, Fort Worth, Texas, May 1995.
 11. Splettstoesser, W. R., Schultz, K. J., van der Wall, B. G., Buchholz, H., Gemblar, W. and Niesl, G., "The Effect of Individual Blade Control on BVI Noise-Comparisons of Flight Test and Simulation Results", Proceedings of 24th European Rotorcraft Forum, Marseilles, France, 1998.
 12. Bebesel, M., Roth, D., Pongratz, R., "Reduction of BVI Noise on Ground- In-Flight Evaluation of Closed-Loop Controller", 28th European Rotorcraft Forum, Bristol, United Kingdom, September 2002.
 13. Jacklin, S. A., Haber A., de Simone G., Norman, T. R., Shinoda P., "Full-Scale Wind Tunnel Test of an Individual Blade Control System for a UH-60 Helicopter", Proceedings of the 58th Annual Forum of the American Helicopter Society, Montreal, Canada, June, 2002.
 14. Booth, E. R. Jr. and Wilbur, M. L., "Acoustic Aspects of Active-Twist Rotor Control", Proceedings of the 58th Annual Forum of the American Helicopter Society, Montreal, Canada, June, 2002.
 15. Marcolini, M. A., Booth, E. R. Jr., Tadghighi, H., Hassan, A. A., Smith, C. D., and Becker, L. E., "Control of BVI Noise Using an Active Trailing Edge Flap". American Helicopter Society Vertical Lift Aircraft Design Conference, San Francisco, CA 1995.
 16. Kobiki, N., Tsuchihashi, A., Murashige, A., and yamakawa, E., "Study for the Effect of Active Flap on Blade-Vortex Interaction", Heli Japan, 98, Gifu, Japan, 1998.
 17. Shen, J., and Chopra, I., "Aeroelastic Modeling of Trailing-Edge Flap for Helicopter Rotors", Proceedings of 41st AIAA SDM Conference, AIAA-2000-1622, Atlanta, GA, April 2001.
 18. Liu, L., Patt, D., and Friedmann, P. P., "simultaneous Vibration and Noise Reduction in Rotorcraft Using Aeroelastic Simulation", Proceedings of the 60th Annual Forum of the American Helicopter Society, Baltimore, MD, June 2004.
 19. Patt, D., Liu, L., and Friedman, P. P., "Active Flaps for Noise Reduction: A Computational Study", Proceedings of the Society 61st Annual Forum of the American Helicopter, Grapevine, Texas, June 2005.
 20. Koratkar, N. A., and Chopra, I., "Wind Tunnel Testing of a Mach-scaled Rotor Model with Trailing Edge Flaps", Proceedings of the 57th Annual Forum of the American Helicopter Society, Washington DC, May 2001.
 21. Hasegawa, Y., Katayama, N., Kobiki, N., Nakasato, E., Yamakawa, E., and Okawa, H., "Experimental and Analytical Results of Whirl Tower Test of ATIC Full-Scale Rotor System", Proceedings of the 57th Annual Forum of the American Helicopter Society, Washington DC, May 2001.
 22. Enenkl, B., Kloppel, V., Preiler, D., and Janker, P., "Full-Scale Rotor with Piezoelectric Actuated Blade Flaps", 28th European Rotorcraft Forum, Bristol, United Kingdom, September 2002.
 23. Kloppel, V., and Enenkel, B., "Rotor Blade Control by Active Servo Flaps", International Fom on Aeroelasticity and Structural Dynamics 2005-04-21, Muenchen, Germany, June 28-July 1, 2005.
 24. Konstanzer, P. et al., "Recent Advances in Eurocopter's passive and active vibration control," Proceedings of the 64th Annual Forum of the American Helicopter Society, Montreal, Canada, April 29-May 1, 2008.
 25. Straub, F. K., and Kennedy, D. K., "Design, Development, Fabrication and Testing of an Active Flap Rotor System", Proceedings of the 61st Annual Forum of the American Helicopter Society, Grapevine, Texas, June 2005.
 26. Straub, F. K., and Hassan, A. A., "Aeromechanic Considerations in the Design of a Rotor with Smart Material Actuated Trailing Edge Flaps," Proceedings of the 52nd Annual Forum of the American Helicopter Society, Washington DC, June 1996.
 27. Straub, F. K., Vaidyanathan, A. R., Birchette, T., and Lau, B. H., "Wind Tunnel Test of the SMART Active Flap Rotor", Proceedings of the 65th Annual Forum of the American Helicopter Society, Grapevine, Texas, May 27-29, 2009.
 28. Jacklin, S. A., Lau, B. H., Nguyen, K. Q., Smith, R. L. and McNulty, "Full-Scale Wind Tunnel Test of the McDonnell Douglas Five-Bladed Advanced Bearingless Rotor: Performance, Stability, Loads, Control Power, Vibration and HHC Data," Presented at the American Helicopter Society Aeromechanics Specialists Conference, San Francisco, California, January 19-21, 1994.
 29. Sim, B. W., JanakiRam, R. D., Barbely, N. L., Solis, E., "Reduced In-Plane Low Frequency Noise of an Active Flap Rotor", Proceedings of the 65th Annual Forum of the American Helicopter Society, Grapevine, Texas, May 27-29, 2009.
 30. Schmitz, F. H., Allmen, J. R., and Soderman, P. T., "Modification of the Ames 40- by 80-Foot Wind Tunnel for Component Acoustic Testing for the Second

Generation Supersonic Transport,” NASA TM-108850, October 1994.

31. Soderman, P. T., Jaeger, S. M., Hayes, J. A. and Allen, C. S., “Acoustic Quality of the 40- by 80-Foot Wind Tunnel Test Section After Installation of a Deep Acoustic Lining,” NASA TP-2002-211851, November 2002.
32. Allen, C. S., Jaeger, S. M. and Soderman, P. T., “Background Noise Sources and Levels in the NASA Ames 40- by 80-Foot Wind Tunnel at the Turn of the Century: A Status Report,” NASA TP-2003-212259, November 2003.
33. Johnson, W. R., “Rotorcraft Aerodynamics Models for a Comprehensive Analysis,” Proceedings of the 54th Annual Forum of American Helicopter Society, Washington, D.C., May 1998.
34. Yeo, H. S. and Johnson, W. R., “Assessment of Comprehensive Analysis Calculation of Airloads on Helicopter Rotors,” *Journal of Aircraft*, Vol. 42, No. 5, September-October 2005, pp. 1218 – 1228.
35. Kottapalli, S. and Straub, F. K., “Correlation of SMART Active Flap Rotor Loads,” ”, Proceedings of the 65th Annual Forum of the American Helicopter Society, Grapevine, Texas, May 27-29, 2009.
36. Shirey, J. S., Brentner, K. S., Chen, H.-N., “A Validation Study of the PSU-WOPWOP Rotor Noise Prediction System,” 45th AIAA Aerospace Sciences Meeting and Exhibit, Reno, Nevada, January 8-11, 2007.
37. Hall, Steven R., Straub, Friedrich K. and Vaidyanathan, Anand R., “Active Flap Control of the SMART Rotor for Vibration Reduction” Proceedings of the 65th Annual Forum of the American Helicopter Society, Grapevine, Texas, May 27-29, 2009.
38. Lim, J. W., Nygaard, T. A., Strawn, R., and Potsdam, M., “Blade-Vortex Interaction Airloads Prediction Using Coupled Computational Fluid and Structural Dynamics,” *Journal of the American Helicopter Society*, Vol. 52, (4), October 2007, pp. 318-328
39. Sim, B. W. and Lim, J. W., “Blade-Vortex Interaction (BVI) Noise & Airload Predictions Using Lose Aerodynamic/Structural Coupling,” Proceedings of 62nd Annual Forum of the American Helicopter Society, Phoenix, Arizona, May 2006.
40. Boyd Jr., D., “HART-II Acoustic Predictions using a Coupled CFD/CSD Method”, Proceedings of the 65th Annual Forum of the American Helicopter Society, Grapevine, Texas, May 27-29, 2009.